JOURNAL OF PETROLOGY | VOLUME 47 | NUMBER 5 | PAGES 929–964 | 2006 | doi:10.1093/petrology/egi101

Petrology and Geochemistry of Eclogite Xenoliths from the Colorado Plateau: Implications for the Evolution of Subducted Oceanic Crust

TOMOHIRO USUI[1]*, EIZO NAKAMURA[1] AND HERWART HELMSTAEDT[2]

[1]PHEASANT MEMORIAL LABORATORY FOR GEOCHEMISTRY AND COSMOCHEMISTRY, INSTITUTE FOR STUDY OF THE EARTH'S INTERIOR, OKAYAMA UNIVERSITY AT MISASA, TOTTORI, 682-0193, JAPAN

[2]DEPARTMENT OF GEOLOGICAL SCIENCES AND GEOLOGICAL ENGINEERING, QUEEN'S UNIVERSITY, KINGSTON, ONT., K7L 3N6, CANADA

RECEIVED DECEMBER 9, 2004; ACCEPTED DECEMBER 19, 2005
ADVANCE ACCESS PUBLICATION FEBRUARY 21, 2006

Eclogite xenoliths from the Colorado Plateau, interpreted as fragments of the subducted Farallon plate, are used to constrain the trace element and Sr–Nd–Pb isotopic compositions of oceanic crust subducted into the upper mantle. The xenoliths consist of almandine-rich garnet, Na-clinopyroxene, lawsonite and zoisite with minor amounts of phengite, rutile, pyrite and zircon. They have essentially basaltic bulk-rock major element compositions; their Na_2O contents are significantly elevated, but K_2O contents are similar to those of unaltered mid-ocean ridge basalt (MORB). These alkali element characteristics are explained by spilitization or albitization processes on the sea floor and during subduction-zone metasomatism in the fore-arc region. The whole-rock trace element abundances of the xenoliths are variable relative to sea-floor-altered MORB, except for the restricted Zr/Hf ratios (36·9–37·6). Whole-rock mass balances for two Colorado Plateau eclogite xenoliths are examined for 22 trace elements, Rb, Cs, Sr, Ba, Y, rare earth elements, Pb, Th and U. Mass balance considerations and mineralogical observations indicate that the whole-rock chemistries of the xenoliths were modified by near-surface processes after emplacement and limited interaction with their host rock, a serpentinized ultramafic microbreccia. To avoid these secondary effects, the Sr, Nd and Pb isotopic compositions of minerals separated from the xenoliths were measured, yielding 0·70453–0·70590 for $^{87}Sr/^{86}Sr$, −3·1 to 0·5 for εNd and 18·928–19·063 for $^{206}Pb/^{204}Pb$. These isotopic compositions are distinctly more radiogenic for Sr and Pb and less radiogenic for Nd than those of altered MORB. Our results suggest that the MORB-like protolith of the xenoliths was metasomatized by a fluid equilibrated with sediment in the fore-arc region of a subduction zone and that this metasomatic fluid produced continental crust-like isotopic compositions of the xenoliths.

KEY WORDS: *Colorado Plateau; eclogite xenolith; geochemistry; subducted oceanic crust*

INTRODUCTION

Material recycling through subduction zones is one of the most important processes controlling the chemical evolution of the Earth, and materials from the Earth's surface are likely to have been reintroduced into its interior throughout geological history. Although most of the subducting plate is made of mantle material returning to depths from which it originated, hydrated and altered upper oceanic crust, as well as overlying sediments, carry a record of low-temperature interactions with continents, oceans and the atmosphere into the deep mantle. Subduction of surface and near-surface components can change the volatile contents, trace element abundances, amounts of heat-producing elements and radiogenic isotope systematics in the mantle.

A number of geochemical models have been developed to estimate the integrated trace element and isotopic

*Corresponding author. Present address: Department of Earth and Planetary Sciences, University of Tennessee, 1412 Circle Drive, Knoxville, TN 37996, USA. Telephone: +1-865-974-3874. Fax: +1-865-974-2368. E-mail: tusui@utk.edu

composition of a hypothetical slab-derived 'component' in arc and ocean island basalt (OIB) lavas (e.g. Zindler & Hart, 1986; McCulloch & Gamble, 1991; Ishikawa & Nakamura, 1994; Hofmann, 1997; Taylor & Nesbitt, 1998; Stracke *et al.*, 2003). However, contributions from individual sources are difficult to assess from lava compositions alone, because element fractionations during slab dehydration and mass fluxes from the various subducted 'lithologies' are poorly constrained. Nevertheless, most models have used a geochemical 'component' estimated from rock compositions prior to subduction (e.g. samples from ocean-floor drilling). Therefore, understanding the trace element and isotopic compositions of individual rock types subducted into the sub-arc mantle is indispensable for constraining geochemical models for subduction-zone material recycling.

One approach to constrain material cycling involves high-pressure experimental studies that simulate processes such as dehydration of the subducting slab under controlled conditions (e.g. Schmidt & Poli, 1998; Okamoto & Maruyama, 1999; Poli & Schmidt, 2002). Such experiments provide important constraints on the water contents and metamorphic phase relations in the subducting slab as a function of temperature and pressure. Other experiments have investigated the solubility of elements in fluids at high pressures, as well as element partitioning between the fluids and the constituent minerals in potential slab materials such as eclogites, blueschists and serpentinites (e.g. Brenan *et al.*, 1994, 1995, 1998; Iizuka & Nakamura, 1995; Ayers *et al.*, 1997; Kogiso *et al.*, 1997; Stalder *et al.*, 1998). However, microanalytical and mass balance studies of subduction-related metamorphic rocks have shown that many so-called trace elements are preferentially partitioned into accessory minerals such as allanite, rutile, apatite, and zircon, and that elemental partitioning commonly does not reach equilibrium because of the relatively low-temperature environment envisaged in the subducting oceanic lithosphere (e.g. Sorensen & Grossman, 1989, 1993; Sorensen, 1991; Tribuzio *et al.*, 1996; Zack *et al.*, 2002*a*, 2002*b*; Spandler *et al.*, 2003). This suggests that partition coefficient data for trace elements may not be appropriate for evaluating trace element behaviors in subducting oceanic crust.

Thermomechanical studies indicate that subducting oceanic crust in cold subduction zones passes through the blueschist to lawsonite eclogite transition, and that the most important dehydration process for inducing island arc volcanism occurs in the lawsonite eclogite facies (Peacock, 1993). Thus, lawsonite eclogites are critical to investigating trace element and isotopic behavior in subducted oceanic crust. However, data for trace element distributions among the mineral assemblages in the lawsonite eclogite facies are limited, because lawsonite eclogite terranes are rare (Zack *et al.*, 2004), and commonly much overprinted by high-T/P retrogression.

Lawsonite-bearing eclogite xenoliths from the Colorado Plateau of the southwestern USA present an important opportunity to study the trace element and isotopic systematics of this lithology. Helmstaedt & Doig (1975) showed that these xenoliths resemble eclogites of the Franciscan Complex of the California Coast Ranges, western USA, in many aspects of their petrography and geochemistry. The Franciscan Complex represents fragments of a fossil subduction-zone plate boundary from the Jurassic to the Paleogene (e.g. Ernst, 1970; Maruyama & Liou, 1989). Offshore magnetic anomalies demonstrate that thousands of kilometers of oceanic crust have been subducted beneath the western US continental margin since the Late Cretaceous (Hamilton, 1969). Usui *et al.* (2003) used ion microprobe techniques to determine the U–Pb ages of zircons from the Colorado Plateau eclogite xenoliths, which yielded concordant ages from 81 to 33 Ma. Those workers interpreted the two extremes in age to reflect zircon crystallization during subduction-related metamorphism and zircon recrystallization during intrusion of the host rock. Combining geotectonic reasoning with the zircon geochronology and petrographic similarities to subduction-related eclogites led Usui *et al.* (2003) to conclude that the Colorado Plateau eclogite xenoliths originated as fragments of the subducted Farallon plate that had resided in the upper mantle since the Late Cretaceous. Owing to their rapid transport to the surface, the eclogite xenoliths show few effects of retrograde overprinting compared with crustal eclogites exhumed by tectonic processes. Thus, they may preserve important chemical information about their subduction-related metamorphic history.

Two problematic issues remain concerning the origin of the Colorado Plateau eclogite xenoliths. One is whether they represent fragments of relatively young Phanerozoic subducted oceanic crust (Helmstaedt & Doig, 1975; Usui *et al.*, 2003) or remnants of the much older, Proterozoic basement of the Colorado Plateau (Roden *et al.*, 1990; Wendlandt *et al.*, 1993; Smith *et al.*, 2004). The contrasting hypotheses for their ages may be considered to result, in part, from the application of different geochronological methods to date them. U–Pb zircon ages by ion microprobe analysis have yielded Phanerozoic ages (Usui *et al.*, 2003), whereas Sm–Nd isotopic data (Roden *et al.*, 1990; Wendlandt *et al.*, 1993) give Proterozoic model ages in the range of 1500–1800 Ma. In addition, U–Pb analyses of multigrain zircon fragments by the isotope dilution method with thermal ionization mass spectrometry (ID-TIMS) resulted in a linear discordant line that intersected the concordia at 1514 Ma (Smith *et al.*, 2004).

The other debated issue is whether the Colorado Plateau eclogite xenoliths were formed by prograde metamorphism during subduction of oceanic lithosphere or by magmatic recrystallization processes in the upper mantle. Based on mineral textures and compositional zoning of garnet and clinopyroxene, Helmstaedt & Schulze (1988, 1991) concluded the former. They estimated two metamorphic temperatures for the eclogite xenoliths, corresponding to crystallization of garnet cores and peak metamorphic conditions, respectively, and concluded that the garnet rims formed at ~100°C higher temperatures than the garnet cores. However, these estimates are unlikely to be conclusive because: (1) they depend on calculating the Fe^{2+}/Fe^{3+} of clinopyroxene, a parameter that cannot be determined by electron microprobe; (2) it is difficult to determine the clinopyroxene core–garnet core temperature by using clinopyroxene with an oscillatory zoned structure. Smith & Zientek (1979) suggested that the oscillatory zoning of clinopyroxene may represent disequilibrium growth in the presence of fluid phases, and that the Colorado Plateau eclogite xenoliths formed coexisting with a fluid phase during cooling and metasomatism of basaltic dikes in a cool upper mantle.

In this paper, we report whole-rock and mineral data for major, minor, and trace elements, and Sr, Nd, and Pb isotopic data for a suite of Colorado Plateau eclogite xenoliths. The geochemical data are complemented by observations of the modes of constituent minerals, their textures and chemical zoning structures. We reassess the contrasting hypotheses for the origin of the Colorado Plateau eclogite xenoliths and demonstrate that these rocks can be used as proxies to understand the geochemical evolution of subducted oceanic crust. These data allow us to develop a model for the trace element and isotopic (Sr, Nd and Pb) composition of subducted oceanic crust in the sub-arc region.

GEOLOGICAL SETTING

The Colorado Plateau is a broadly elevated region, ~1500 m above sea level, in the southwestern interior of the USA. Unmetamorphosed and little deformed Paleozoic to Cenozoic sedimentary rocks are well exposed on Precambrian basement (1·4–1·8 Ga; Condie, 1982). The plateau is surrounded by the Basin and Range, Rocky Mountains, and the Rio Grande Rift tectonic provinces, all of which have experienced intense Cenozoic orogenic activity and extensional tectonics (Fig. 1a). The structure of the Colorado Plateau consists of broad basins, uplifts and platforms, which are locally bordered by monoclines. Tectonic reconstruction of the history of the western margin of North America suggests that during the Late Cretaceous and Early Tertiary, the Farallon plate was subducting eastward (Atwater, 1970). The Late Cretaceous and Tertiary records of arc magmatism in the southwestern USA constrain the slab geometry and its evolution, suggesting that the migration of arc magmatism was probably caused by progressive flattening of a subducting slab (Coney & Reynolds, 1977). Intra-plate magmatism, which occurred extensively around the Colorado Plateau, may be associated with the formation of a slab window and/or slab tearing (Dickinson, 1997).

Eight diatremes of serpentinized ultramafic microbreccia and numerous minette diatremes, the products of intra-plate magmatism, are exposed in the Navajo Volcanic Field of the Colorado Plateau (Fig. 1b). The microbreccia diatremes occur as two structurally controlled clusters (McGetchin *et al.*, 1977). One, related to the Comb Ridge monocline on the eastern margin of Monument uplift, includes the Mule Ear, Moses Rock, Cane Valley, and Garnet Ridge diatremes. The other, at the eastern margin of the Defiance uplift, includes the Buell Park and Green Knobs diatremes. A single diatreme, Red Mesa, lies between the two fields and is located about 30 km east of the Comb Ridge monocline.

The diatreme rocks that host the eclogite xenoliths lack primary igneous textures and consist of finely crushed fragments of strongly serpentinized ultramafic rocks. Although initially described as kimberlites (e.g. McGetchin *et al.*, 1977), these rocks are not 'true' kimberlites (e.g. Clement *et al.*, 1984) but serpentinized ultramafic microbreccias (SUM; Roden, 1981). The microbreccia diatremes were emplaced between 25 and 35 Ma (Naeser, 1971; Helmstaedt & Doig, 1975; Roden *et al.*, 1979), contemporaneous with the numerous minette diatremes of the Navajo Volcanic Field (Ehrenberg, 1982). The diatremes contain several types of eclogite, as well as a broad spectrum of possible upper mantle rocks that include variously hydrated spinel- and garnet-bearing peridotites, pyroxenites and serpentinites. The eclogite xenoliths are found mainly in three microbreccia diatremes in the Comb Ridge cluster (Garnet Ridge, Moses Rock, Mule Ear), and are absent from the Green Knobs and Buell Park pipes near the Defiance uplift (McGetchin *et al.*, 1977; Selverstone *et al.*, 1999). The samples used for this study were collected from the Moses Rock and Garnet Ridge diatremes.

ANALYTICAL METHODS

Major element compositions of minerals were determined using a JEOL JXA-8800 electron microprobe at ISEI (Institute for Study of the Earth's Interior). Analyses were carried out at 15 kV and 20 nA sample current for all silicate minerals. Counting times of 30 s were used, and matrix corrections were performed by ZAF methods. The standards are synthetic oxides and natural minerals. The modal abundance of zircon was determined by

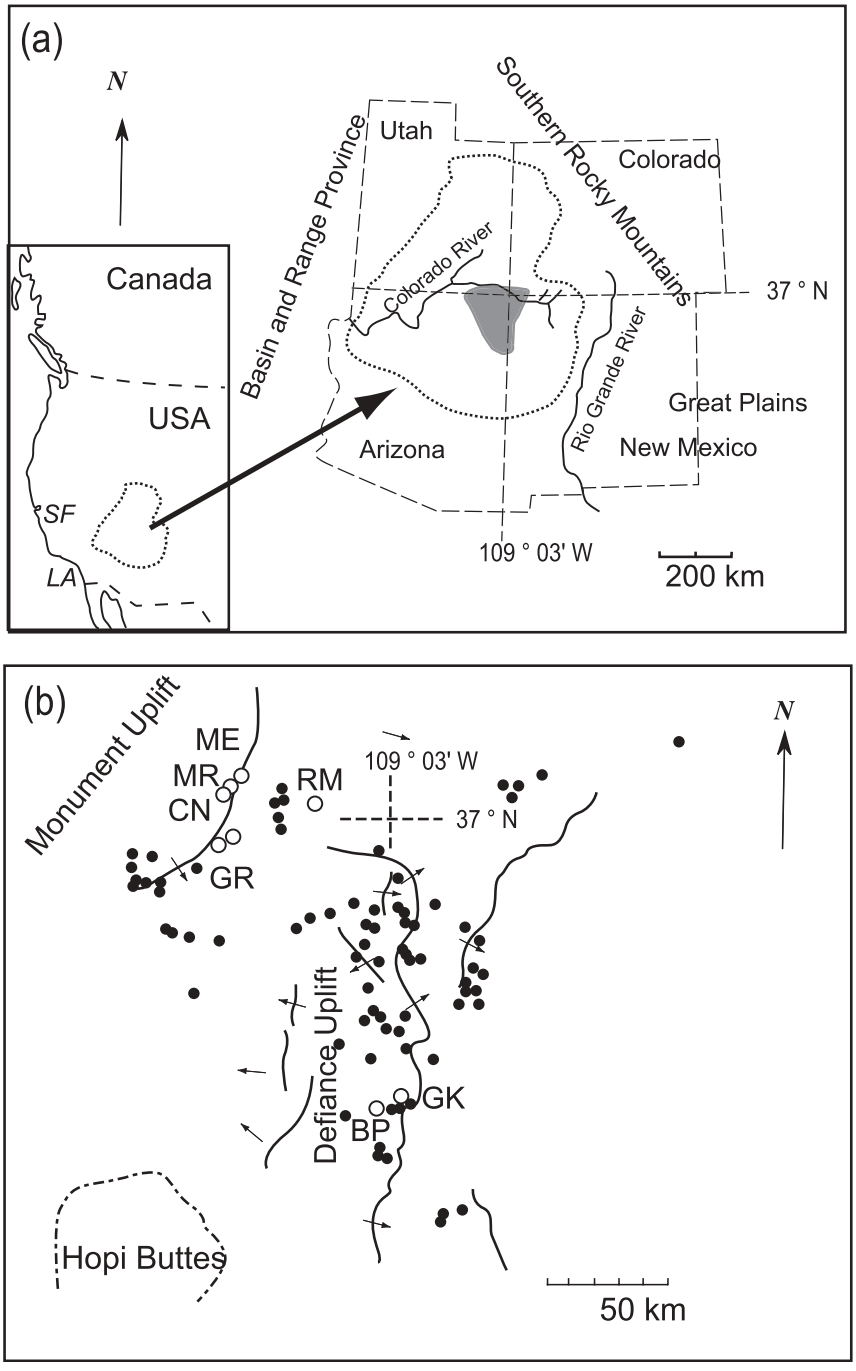

Fig. 1. (a) Sketch map of the southwestern interior of the USA and outline of the Colorado Plateau (dotted line). (b) Sketch map of the Navajo Volcanic Field in the Colorado Plateau near the Four Corners shown as the gray shaded area in (a), modified after Smith & Levy (1976). ●, minettes; ○, serpentinized ultramafic microbreccia diatremes. Major monoclines with dip directions are also shown. ME, Mule Ear; MR, Moses Rock; CN, Cane Valley; GR, Garnet Ridge; RM, Red Mesa; BP, Buell Park; GK, Green Knobs; SF, San Francisco; LA, Los Angeles.

digital image analysis of 25 randomly selected back-scattered electron images (each 1000 μm) per sample.

Trace element analyses of garnet, clinopyroxene, lawsonite and zoisite were performed using a CAMECA ims-5f ion microprobe at the PML (Pheasant Memorial Laboratory) in the ISEI, using techniques described by Nakamura & Kushiro (1998). Clinopyroxene from mantle xenoliths and basaltic natural glass were used as standard minerals for trace element calibrations. Trace element concentrations in these standards were

chemically determined by inductively coupled plasma mass spectrometry (ICP-MS; Makishima & Nakamura, 1997). The homogeneity of these standards was confirmed by optical microscope, electron microprobe and ion microprobe analysis. Trace element contents of garnet and clinopyroxene were calibrated on the basis of the clinopyroxene standard, and those of lawsonite and zoisite were calibrated using the basaltic glass standards. Minerals in thin sections were sputtered with an O^- primary beam of 10–20 nA intensity, resulting in 10–20 μm beam diameter. Clinopyroxene and lawsonite inclusions <30 μm in diameter were measured by an O^- primary beam of ~6 nA intensity, which produced a beam <10 μm in diameter. Positive secondary ions were collected by ion counting using an energy offset of −60 V from 4500 V acceleration with an energy bandpass of ±10 V. These operating conditions resulted in $(1–1{\cdot}5) \times 10^5$ c.p.s. for ^{30}Si secondary ions. The secondary ion intensities of atomic masses of interest were normalized to ^{30}Si. For each analysis spot, 15 trace elements were determined in a run that took ~40 min, including presputtering. The analytical reproducibility (relative standard deviation % for $n = 10$) for trace element measurements is generally <10% for the clinopyroxene standard and <5% for the basaltic glass standard, except for Er and Lu (7–10%).

To prepare whole-rock powders for analysis, eclogite samples were broken into chips ~2 mm in diameter. Fresh pieces were hand-picked and washed with deionized water in an ultrasonic bath for 30 min. After drying at 60°C overnight, the chips were pulverized using a silicon nitride triturator to a grain size <400 mesh. To separate minerals, rock powders obtained using the silicon nitride triturator were sieved to capture grain sizes between 80 and 100 mesh (an average grain size of ~200 μm). This sieved fraction was processed with an isodynamic separator, and the resulting mineral fractions were hand-picked.

Whole-rock major element compositions, along with Cr and Ni, were determined by X-ray fluorescence (XRF) spectrometry at the PML, on glass beads fluxed from mixing 100 mg of powdered sample and 5 g of lithium tetraborate (Takei, 2002). Trace element compositions were measured by ICP-MS at the PML, based on the methods of Makishima & Nakamura (1997) for Y, Cs, Ba, rare earth elements (REE), Pb, Th and U, those of Makishima *et al.* (1999) for Zr, Hf and Nb, and of Moriguti *et al.* (2004) for Li. Powdered samples (20 mg) for ICP-MS analysis were decomposed in 1·0 ml of HF and 0·1 ml of HNO_3 in Teflon bombs at 210°C for 2 days, because acid-resistant minerals such as zircon and rutile are present in the eclogite samples. Analytical errors for trace element were generally 3% for Zr, Hf, and Li, and 5% for other elements.

The analytical procedures for mass spectrometry followed Yoshikawa & Nakamura (1993) for Sr isotopic ratios and abundances of Rb and Sr, Makishima & Nakamura (1991) for Nd isotopic ratios and abundances of Sm and Nd, Kuritani & Nakamura (2002, 2003) for Pb isotopic ratios and Pb abundances, and Yokoyama *et al.* (1999, 2003) for abundances of U and Th, employing TIMS in static multi-collection mode [modified Finnigan MAT261: 'Kiji' (Nakano & Nakamura, 1998), MAT262: 'Taro' and MAT262: 'INU']. All of these elements (Rb, Sr, Sm, Nd, U, Th and Pb) were successively separated from each of the whole-rock and mineral samples, using a multi-ion exchange column chemistry approach modified after Nakamura *et al.* (2002).

Basaltic standard JB3 from the Geological Survey of Japan (GSJ) yields typical analytical reproducibility of 0·005%, 0·005% and 0·02% for Sr, Nd and Pb isotopic ratios, respectively, and <1% for Rb, Sr, Sm, Nd, U, Th and Pb abundances. Accuracies of the isotopic and concentration analyses were confirmed by repeated measurement of JB3. We obtained data for this standard consistent with the previously published data within the analytical reproducibility (see Appendix, Table A1). Isotopic fractionation during analysis was corrected using $^{86}Sr/^{88}Sr = 0{\cdot}1194$ and $^{146}Nd/^{144}Nd = 0{\cdot}7219$ as normalizing factors. Pb isotopic fractionation was corrected by the 'two-double spikes method' with ^{205}Pb–^{204}Pb and ^{207}Pb–^{204}Pb enriched spikes following the technique of Kuritani & Nakamura (2003). The composition of the spike was calibrated by assuming that the $^{208}Pb/^{206}Pb$ ratio of NBS982 is 1·00016 (Catanzaro *et al.*, 1968). Instrumental mass discrimination of TIMS analyses was corrected by the following values of standards: $^{87}Sr/^{86}Sr = 0{\cdot}71024$ (NIST987), $^{143}Nd/^{144}Nd = 0{\cdot}511839$ (La Jolla), and $^{206}Pb/^{204}Pb = 16{\cdot}9424$, $^{207}Pb/^{204}Pb = 15{\cdot}5003$, $^{208}Pb/^{204}Pb = 36{\cdot}7266$ (NBS981).

RESULTS

Mineral assemblage and classification of eclogite xenoliths

The Colorado Plateau eclogite xenoliths investigated in this study were previously described and referred to as metabasic eclogite and jadeite-clinopyroxenite, based not only on their mineral assemblages and basaltic bulk compositions, but also on their textural similarity to crustal examples of eclogites (Helmstaedt & Schulze, 1988). In this paper, 'jadeitic'-clinopyroxenite is used instead of jadeite-clinopyroxenite, because clinopyroxene in this xenolith type is not pure jadeite, but omphacite or impure jadeite as described later. The mineral assemblages of the xenoliths and their modal proportions are given in Tables 1 and 2.

Table 1: Mineral assemblages of Colorado Plateau xenoliths

Rock type	Sample	Grt	Cpx	Lw	Zo*	Rut	Phen	Pyrite	Zir	Ap	Coe	Albite*	Barite*	Chlorite*	Limonite*	Others
Lw-Ec	GR1	+	+	+	+	+	+		—		—		—			$CuFeS_2$
Zo-Ec	MR4	+	+		+	+		+	—				—			
Zo-Ec	MR7	+	+	—	+	+			—	+	—		—		—	orthoclase
Zo-Ec	MR15	+	+		+	+		+	—				—		—	
Zo-Ec	MR19	+	+		+	+			—				—		—	
Zo-Ec	MR49	+	+		+	+		+	—				—		—	
Zo-Ec	MR29	+	+		+	+		+	—				—			
Jd-Cl	MR26	+	+		+	+		+	—			—	—			
Jd-Cl	MR21	+	+		+	+	+	+	—			—	—			
Jd-Cl	MR3B	+	+		+	+	+	+	—			—	—	—	—	paragonite
Jd-Cl	MR50	+	+			+		+	—			—	—		—	
Jd-Cl	MR47	—	+			+		+	—			—	—			

*Retrograde overprinting.
Lw-Ec, lawsonite-eclogite; Zo-Ec, zoisite-eclogite; Jd-Cl, jadeitic-clinopyroxenite; +, major constituent (>0·1%); —, minor constituent (<0·1%); Grt, garnet; Cpx, clinopyroxene; Lw, lawsonite; Zo, zoisite; Rut, rutile; Coe, coesite; Phen, phengite; Ap, apatite; Zir, zircon.

Table 2: Modal proportions (vol. %) in the Colorado Plateau xenoliths

Rock type	Sample	Grt	Cpx	Lw	Zo	Rut	Phen	Pyrite	Ap	Total points	*Zir*
Lw-Ec	GR1	24·8	59·0	6·6	7·6	1·6	0·1			8249	*0·040**
Zo-Ec	MR4	25·8	30·4		39·7	0·9		1·7		2000	*0·012**
Zo-Ec	MR7	19·2	57·5	<0·1	21·8	0·9		<0·1	0·4	4572	*0·008**
Zo-Ec	MR15	11·6	66·0		20·2	0·7		1·1		2535	
Zo-Ec	MR19	27·2	49·5		20·2	3·2		<0·1		2000	
Zo-Ec	MR49	7·6	77·3		12·2	1·3		1·1		3000	
Zo-Ec	MR29	23·2	45·0		29·1	2·3		0·4		2856	
Jd-Cl	MR26	13·4	76·5		7·2	2·3		0·6		3000	
Jd-Cl	MR21	14·0	79·6		3·0	1·5	0·9	1·0		3000	
Jd-Cl	MR3B	25·1	69·0		0·3	0·9	3·8	0·8		2895	*0·007**
Jd-Cl	MR50	3·2	93·8		<0·1	1·6		1·4		3000	
Jd-Cl	MR47	<0·1	97·1		<0·1	1·2		1·7		3000	

*Modal proportions of zircon in the xenoliths were determined by digital image analysis. Details are described in the text. Abbreviations as in Table 1.

Metabasic eclogites consist mainly of various proportions of almandine-rich garnet and omphacitic clinopyroxene with some lawsonite and zoisite (Fig. 2). They are either lawsonite-eclogite or zoisite-eclogite, according to the major constituent mineral assemblages (Table 1). Zoisite-eclogite is distinguished from lawsonite-eclogite only by its lack of lawsonite, although trace amounts of lawsonite crystals occur as small (~10 μm) inclusions in garnet in zoisite-eclogites (Fig. 3c). With a decrease in garnet content (approximately <10 vol. %) and an increase of the jadeite component in the clinopyroxene (approximately >70 mol %), the metabasic eclogites grade continuously into jadeitic-clinopyroxenites. Other minerals that occur in trace amounts in both xenolith types are phengite, pyrite, rutile, zircon and apatite. Rare chlorite, albite and barite occur as <5 μm crystals around garnet and clinopyroxene. In both eclogite types, coesite occurs as <20 μm inclusions in garnet crystals, but not in the matrix (Fig. 3a; Usui *et al.*, 2002, 2003).

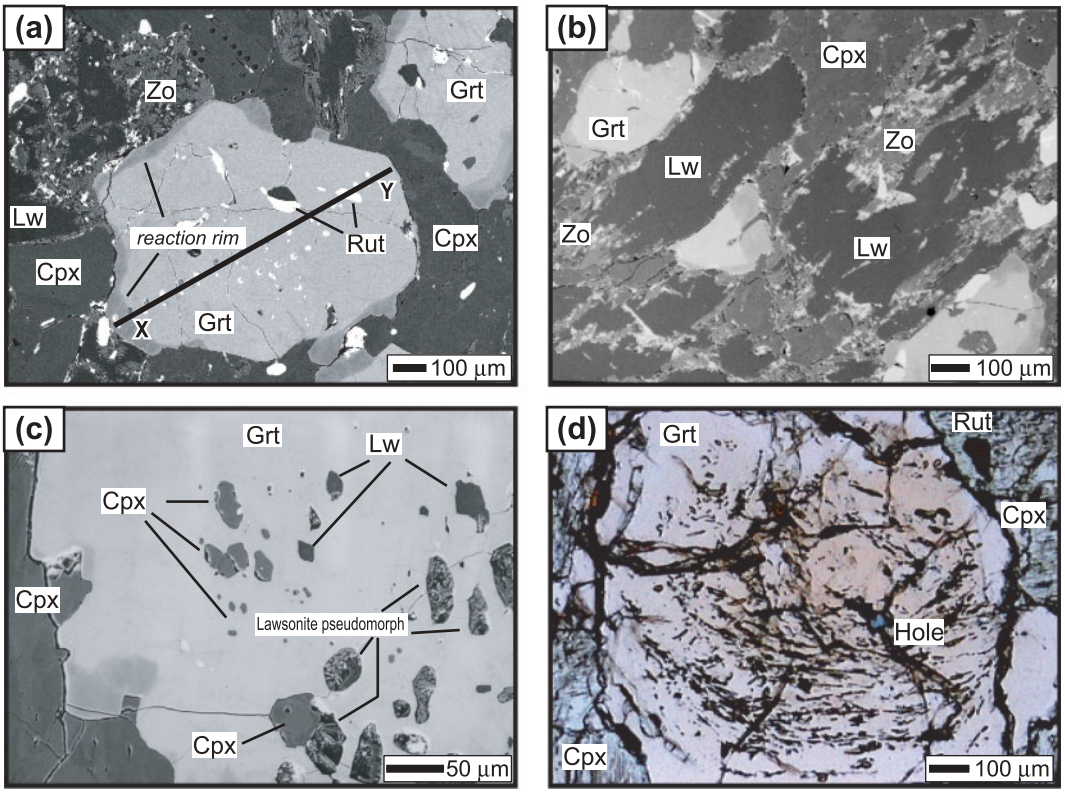

Fig. 2. (a), (b) Back-scattered electron (BSE) image of lawsonite-eclogite GR1. (c) BSE image of included clinopyroxene and lawsonite in GR1. A crack in the lower part of the garnet connects the lawsonite pseudomorphs and an included clinopyroxene to the exterior of the garnet. (d) Photomicrograph (plane-polarized light) of GR1 showing curved trails of inclusions (rutile and coesite) in garnet. Abbreviations are as in Table 1.

Occurrence, textures and compositions of minerals

Garnet

Garnet commonly occurs in small clusters or in thin layers accompanied by lawsonite and zoisite; these generally have euhedral to subhedral outlines with maximum diameters of ~0·1–1·0 mm (Figs 2a and 3a). They are commonly color-zoned, from pink cores to reddish brown rims under plane-polarized light (Fig. 2d). Some grains exhibit rotation textures and contain fine-grained curved inclusion trails of coesite and rutile, indicating that deformation continued after the development of a planar tectonic fabric (Fig. 2d) (see also Helmstaedt & Schulze, 1991).

Garnets have compositions of Alm (Almandine)$_{50–70}$, Sps (Spessartine)$_{<1}$, Pyr (Pyrope)$_{10–30}$, Grs (Grossular)$_{20}$, except for locally developed pyrope-rich rims (Table 3 and Fig. 4). These pyrope-rich rims have distinctively different compositions from the other parts of the garnet, indicating a sharp compositional boundary (Fig. 2a). The compositions of these pyrope-rich rims are about $Alm_{40}Sps_{<1}Pyr_{50}Grs_{10}$ for the lawsonite-eclogite and $Alm_{40}Sps_{<1}Pyr_{40}Grs_{20}$ for the zoisite-eclogite. The rims may have formed under higher temperature conditions when the xenoliths were entrained in the microbreccia host rock, as will be discussed later, and are called 'reaction rims', to distinguish them from 'normal rims' the composition of which is almost identical to those of the core and mantle (Table 4).

In some particularly zoisite-rich eclogites (e.g. MR4, see Table 2), wide reaction rims are present around most garnet crystals, and also penetrate into the garnet cores along cracks (Fig. 3b). The chemical compositions of these garnets in the 'zoisite-rich' eclogites trend toward those of the reaction rims in the (Alm + Sps)–Pyr–Grs diagram (Fig. 4b). In contrast, no reaction rims were observed in jadeitic-clinopyroxenites, which have little or no lawsonite and zoisite, although some garnets have slightly pyrope-rich compositions (Figs 4c and 5a).

The major element compositions of the garnet, except for the reaction rims, are more similar to those from eclogites in subduction-related metamorphic terranes (Low-Temperature eclogite) than to those from diamondiferous kimberlite pipes (High-Temperature eclogite) (Carswell, 1990). The garnets show faint zoning in their Alm, Pyr and Grs components but strong and euhedral zoning in their Sps component, which is

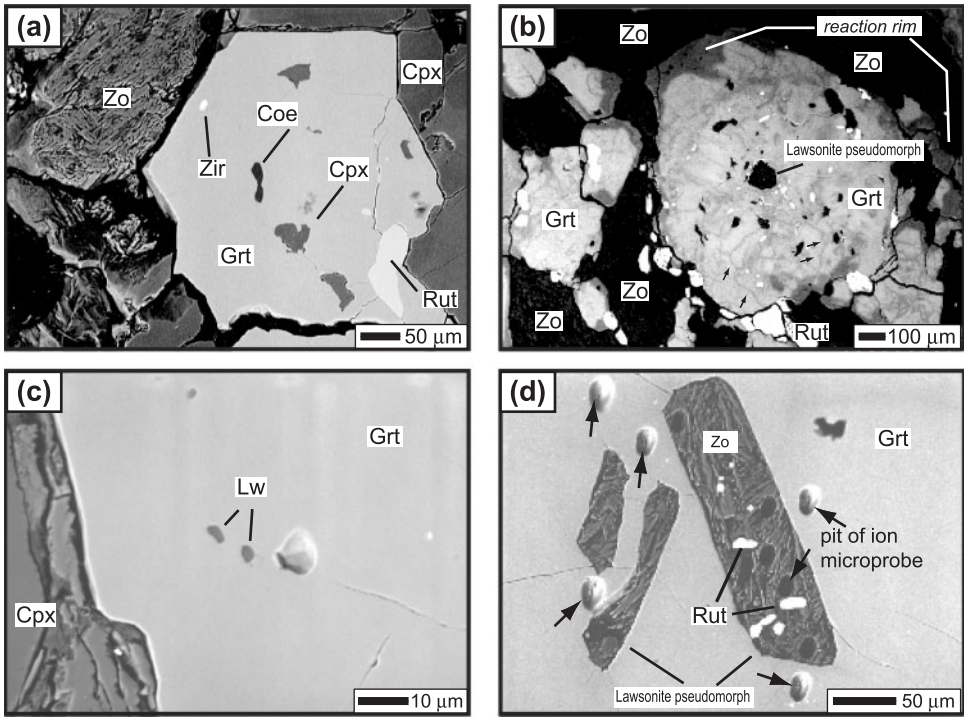

Fig. 3. (a) BSE image of zoisite-eclogite MR7 showing that garnet includes various kinds of inclusions, such as clinopyroxene, coesite, rutile and zircon. (b) High-contrast BSE image of annealed cracks (shown by small arrows) in garnet in zoisite-eclogite MR4. Major element compositions of annealed garnet are similar to that of the reaction rim (see text for details). (c) BSE image of zoisite-eclogite MR7 showing that lawsonite can still survive as inclusions in garnet. (d) BSE image of jadeitic-clinopyroxenite MR3B. Garnet (shown in Fig. 5) includes lawsonite pseudomorphs that are replaced by fibrous zoisite aggregates along with rutile. Cracks connect these lawsonite pseudomorphs. Ion-microprobe pits are indicated by small arrows. Abbreviations are as in Table 1.

much lower than the other three components (Fig. 5). The core is characteristically enriched in Mn relative to the rim.

Clinopyroxene

Clinopyroxene is generally prismatic, and its orientation defines the rock fabric. In thin section it varies in color from colorless to pale green under plane-polarized light. The grain size varies as a result of deformation and synkinematic recrystallization (Helmstaedt & Schulze, 1988). Clinopyroxene grains in the eclogites have compositions near Jd (Jadeite)$_{40–50}$, Aug (Augite)$_{50–60}$, Ac (Acmite)$_{0–8}$, falling into the range of omphacite compositions (Table 4, Fig. 6a and b). On the other hand, clinopyroxenes in the jadeitic-clinopyroxenites have compositions of $Jd_{65}Aug_{20}Ac_{15}$ to $Jd_{75}Aug_{20}Ac_5$. This variation suggests relatively linear jadeite to acmite substitution (Fig. 6c). Clinopyroxene occurs both as inclusions in garnet (referred as 'included clinopyroxene') and in the matrix (referred to as 'matrix clinopyroxene'; Figs 2c and 3a). Included clinopyroxene grains are richer in Ac and poorer in Jd components than matrix clinopyroxene grains, and their composition varies linearly between $Jd_{35}Aug_{50}Ac_{15}$ and $Jd_{40}Aug_{55}Ac_5$ (Fig. 6a and b). This trend is also a jadeite to acmite substitution but it differs from the compositional variations of the matrix clinopyroxene.

Lawsonite and zoisite

Lawsonite is transparent in plane-polarized light. Except for minute inclusions in garnet crystals in the zoisite-eclogite (Fig. 3c), lawsonite is restricted to lawsonite-eclogite. It is invariably rimmed by fine-grained zoisite aggregates (Fig. 2b). Lawsonite grains display relatively uniform compositions close to the ideal formula of $CaAlSi_2O_7(OH)_2{\cdot}H_2O$, with limited substitution of Fe^{3+} for Al and (Na + K) for Ca (Table 5; e.g. Moore & Liou, 1979). Like clinopyroxene, lawsonite occurs both as inclusions in garnet (referred to as 'included lawsonite') and as matrix grains (referred to as 'matrix lawsonite') (Fig. 2b and c). Included lawsonite grains in unfractured garnet crystals lack any rims of zoisite aggregates (Fig. 3c). Most included lawsonites have higher Fe_2O_3 and lower Al_2O_3 contents than matrix lawsonite (Table 5 and Fig. 7).

Zoisite invariably occurs as fine-grained, fibrous and radiating crystal aggregates in eclogite and some jadeitic-clinopyroxenites (Figs 2 and 3). Whereas the zoisite crystals themselves are transparent, the aggregates are dark brown in plane-polarized light. The grain size of

Table 3: Representative electron microprobe analyses of garnet

Rock type:	Lw-Ec			Zo-Ec								Jd-Cl		
Sample:	GR1			MR4			MR7		MR19			MR3B		MR26
Remarks:	core	rim	reaction rim	core	rim	reaction rim	core	rim	core	rim	reaction rim	core	rim	rim
SiO_2	38·52	38·84	40·08	39·12	39·84	40·74	38·08	37·78	38·01	38·35	39·93	37·90	38·77	38·21
TiO_2	0·04	0·02	0·05	0·73	0·06	0·11	0·06	0·00	0·06	0·05	0·00	0·09	0·00	0·00
Al_2O_3	21·84	21·82	22·83	21·00	22·54	22·95	20·79	21·49	20·92	21·44	22·48	20·72	21·61	21·59
Cr_2O_3	0·00	0·01	0·03	0·07	0·03	0·01	0·05	0·02	0·02	0·01	0·03	0·06	0·05	0·03
FeO*	27·07	27·81	20·59	26·39	25·27	18·62	29·48	28·98	27·90	29·64	21·88	31·44	29·93	29·24
MnO	1·49	0·81	0·21	2·09	0·78	0·37	1·44	0·50	3·43	0·65	0·48	1·38	0·10	0·79
MgO	5·58	5·51	12·56	4·98	7·74	10·72	3·28	2·84	2·09	3·98	10·43	2·98	5·72	4·55
CaO	5·82	6·20	4·10	5·97	4·97	7·31	6·89	8·73	8·31	6·20	5·08	4·81	3·80	5·36
Na_2O	0·03	0·00	0·00	0·08	0·03	0·01	0·03	0·00	0·03	0·07	0·01	0·01	0·00	0·03
K_2O	0·00	0·00	0·00	0·00	0·00	0·00	0·00	0·01	0·00	0·01	0·00	0·00	0·00	0·02
NiO	0·02	0·00	0·01	0·02	0·00	0·00	0·01	0·01	0·00	0·01	0·00	0·04	0·00	0·00
Total	100·40	101·02	100·46	100·45	101·25	100·85	100·10	100·35	100·77	100·41	100·33	99·42	99·96	99·82
O.N.	12	12	12	12	12	12	12	12	12	12	12	12	12	12
Si	2·998	3·005	2·985	3·043	3·019	3·019	3·021	2·986	3·013	3·014	3·007	3·037	3·031	3·011
Ti	0·002	0·001	0·003	0·043	0·003	0·006	0·004	0·000	0·003	0·003	0·000	0·005	0·000	0·000
Al	2·003	1·990	2·003	1·924	2·014	2·004	1·944	2·001	1·954	1·986	1·995	1·957	1·991	2·005
Cr	0·000	0·001	0·002	0·004	0·002	0·001	0·003	0·001	0·001	0·001	0·002	0·004	0·003	0·002
Fe^{2+}	1·762	1·799	1·282	1·716	1·602	1·154	1·956	1·916	1·849	1·948	1·378	2·107	1·957	1·927
Mn	0·098	0·053	0·013	0·138	0·050	0·023	0·097	0·033	0·230	0·043	0·031	0·094	0·006	0·053
Mg	0·647	0·636	1·395	0·578	0·874	1·184	0·388	0·335	0·247	0·467	1·171	0·356	0·666	0·534
Ca	0·485	0·514	0·327	0·498	0·403	0·581	0·586	0·740	0·706	0·522	0·410	0·413	0·318	0·452
Na	0·004	0·000	0·000	0·011	0·004	0·002	0·004	0·000	0·005	0·010	0·001	0·002	0·000	0·004
K	0·000	0·000	0·000	0·000	0·000	0·000	0·000	0·001	0·000	0·001	0·000	0·000	0·000	0·002
Ni	0·001	0·000	0·000	0·001	0·000	0·000	0·000	0·001	0·000	0·001	0·000	0·002	0·000	0·000
Cation sum	8·001	7·999	8·010	7·956	7·972	7·974	8·004	8·013	8·009	7·995	7·996	7·978	7·972	7·989
*X*Alm	0·589	0·599	0·425	0·586	0·547	0·392	0·646	0·634	0·610	0·654	0·461	0·710	0·664	0·650
*X*Sps	0·033	0·018	0·004	0·047	0·017	0·008	0·032	0·011	0·076	0·014	0·010	0·032	0·002	0·018
*X*Pyr	0·216	0·212	0·462	0·197	0·298	0·403	0·128	0·111	0·082	0·157	0·392	0·120	0·226	0·180
*X*Grs	0·162	0·171	0·109	0·170	0·138	0·197	0·194	0·245	0·233	0·175	0·137	0·139	0·108	0·153

*Total Fe as FeO.
O.N., oxygen number.

zoisite is generally <10 μm along the major axis and <1 μm along the minor axis, and is much smaller than that of the other constituent minerals, garnet, clinopyroxene, lawsonite, phengite and rutile. It contains 39·7–40·2 wt % SiO_2, 32·6–32·3 wt % Al_2O_3, 23·6–24·2 wt % CaO, and trace amounts of Fe_2O_3, MgO, TiO_2, Na_2O and Cr_2O_3 (Table 5). The textures and major element composition of zoisite are almost identical in lawsonite-eclogite, zoisite-eclogite and jadeitic-clinopyroxenite. Zoisite aggregates also occur as inclusions in fractured garnet preserving the sharp crystal boundaries of euhedral lawsonite pseudomorphs (Fig. 3d), suggesting that the zoisite aggregates originated by replacement of lawsonite.

Other minerals

Phengite occurs in one eclogite (GR1) and two jadeitic-clinopyroxenite (MR21 and MR3B) samples. Grains are platy and up to 0·5 mm in diameter, have relatively homogeneous major element compositions and are characterized by Si values of ~7·5 p.f.u. (per formula unit, O = 22; Table 6). In jadeitic-clinopyroxenite

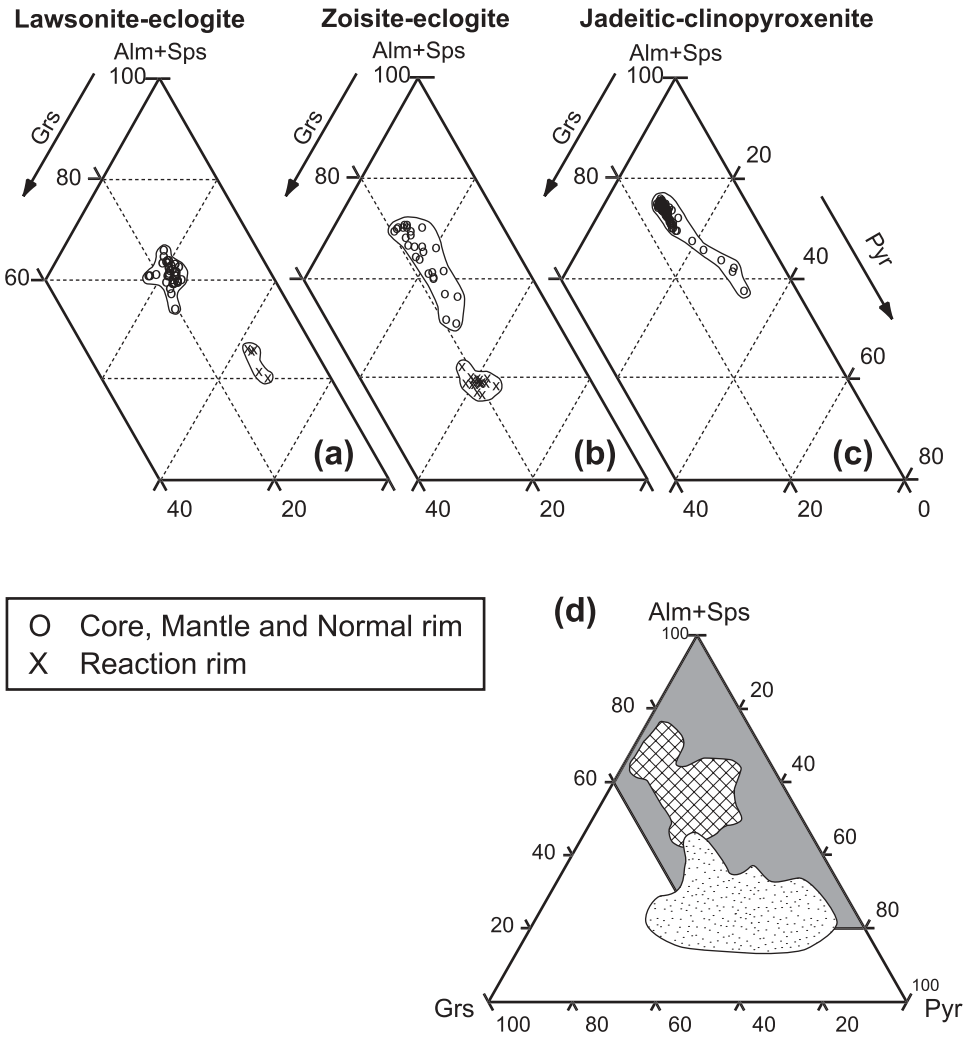

Fig. 4. Composition of garnets in (a) lawsonite-eclogite GR1, (b) zoisite-eclogite MR4 and (c) jadeitic-clinopyroxenite MR3B plotted in the system (Alm + Sps)–Pyr–Grs. The shaded part of the full compositional triangle (d) is enlarged in (a), (b) and (c). Stippled pattern indicates garnets in eclogite xenoliths from diamondiferous kimberlites; cross-hatched pattern, garnets in eclogites from subduction-related metamorphic suites.

samples, albite occurs as a secondary phase along clinopyroxene grain boundaries and rarely along cleavages. The mode of albite is <0·1 vol. %, and it contains <1 % of Or and An components. Orthoclase is present only as inclusions in the core of a garnet from eclogite MR7. Its composition is close to the ideal formula of $KAlSi_3O_8$ (Table 6). Amphibole does not occur in any of our metabasic eclogite xenoliths.

Trace element compositions of minerals

Garnets from eclogites and jadeitic-clinopyroxenites are characterized by extreme LREE (light rare earth element) depletion and HREE (heavy rare earth element) enrichment, exceeding a chondrite-normalized Yb/Ce ratio of 10^4 (Fig. 8). Garnets have REE patterns that appear to increase progressively from La to Dy and are convex-upward from Dy to Lu, except for the reaction rim. The REE patterns of the reaction rims differ in shape from those in other parts of the garnet; they are characteristically convex-upward from La to Dy and concave-downward from Dy to Lu. LREE (La, Ce, Pr and Nd) and MREE (middle rare earth elements: Sm, Eu, Gd and Dy) contents are mostly uniform throughout the crystal, whereas HREE (Er, Yb and Lu) contents are markedly zoned (Fig. 8). The HREE are more abundant in the core relative to the rim, and show a strong correlation with Mn contents (Fig. 9). Garnets in all of the xenoliths are rich in Y, which decreases from core to rim, similar to the HREE (Table 7). Other trace element data for garnet measured by ICP-MS are listed in Table 10.

The clinopyroxenes show two groups of trace element compositions (Fig. 8). The LREE, MREE and Sr contents of clinopyroxenes are higher in eclogite

Table 4: Representative electron microprobe analyses of clinopyroxene

Rock type:	Lw-Ec		Zo-Ec				Jd-Cl		
Sample:	GR1		MR4	MR7		MR19	MR3B	MR26	MR47
Remarks:	matrix	inclusion	matrix	matrix	inclusion	matrix	matrix	matrix	matrix
SiO_2	57·54	57·01	56·67	56·82	54·83	57·19	58·30	56·91	58·20
TiO_2	0·05	0·03	0·06	0·08	0·03	0·02	0·06	0·03	0·09
Al_2O_3	11·04	8·83	11·31	8·99	11·23	12·87	15·43	13·20	16·59
Cr_2O_3	0·04	0·14	0·00	0·01	0·04	0·03	0·04	0·01	0·01
FeO*	2·84	5·96	2·86	7·39	8·25	4·24	5·94	4·14	4·88
MnO	0·04	0·06	0·02	0·07	0·00	0·02	0·09	0·02	0·14
MgO	8·78	8·61	8·63	6·94	5·88	6·48	4·06	6·34	2·86
CaO	12·32	13·08	12·20	12·05	12·37	10·22	5·42	9·84	3·78
Na_2O	7·12	7·17	7·07	7·35	7·36	10·27	11·82	10·35	12·65
K_2O	0·00	0·00	0·00	0·00	0·02	0·02	0·00	0·01	0·01
NiO	0·00	0·00	0·00	0·00	0·00	0·00	0·00	0·02	0·00
Total	99·77	100·88	98·82	99·69	100·01	101·35	101·17	100·85	99·21
O.N.	6	6	6	6	6	6	6	6	6
Si	2·035	2·012	2·022	2·044	1·970	1·964	2·004	1·962	2·026
Ti	0·001	0·001	0·002	0·002	0·001	0·000	0·001	0·001	0·002
Al(IV)	0·000	0·000	0·000	0·000	0·030	0·036	0·000	0·038	0·000
Al(VI)	0·460	0·367	0·476	0·381	0·445	0·485	0·625	0·498	0·681
Cr	0·001	0·004	0·000	0·000	0·001	0·001	0·001	0·000	0·000
Fe*	0·084	0·176	0·085	0·222	0·248	0·122	0·171	0·119	0·142
Mn	0·001	0·002	0·001	0·002	0·000	0·001	0·003	0·000	0·004
Mg	0·463	0·453	0·459	0·372	0·315	0·331	0·208	0·326	0·149
Ca	0·467	0·494	0·466	0·464	0·476	0·376	0·200	0·363	0·141
Na	0·488	0·490	0·489	0·512	0·513	0·683	0·788	0·692	0·854
K	0·000	0·000	0·000	0·000	0·001	0·001	0·000	0·000	0·000
Ni	0·000	0·000	0·000	0·000	0·000	0·000	0·000	0·000	0·000
Total†	4	4	4	4	4	4	4	4	4
Fe^{3+}	0·000	0·093	0·000	0·040	0·095	0·122	0·152	0·119	0·116
Fe^{2+}	0·084	0·083	0·085	0·183	0·152	0·000	0·019	0·000	0·026
Fe^{2+}/Mg	0·181	0·184	0·186	0·491	0·484	0·000	0·093	0·000	0·176
*X*Cats	0·000	0·000	0·000	0·000	0·030	0·038	0·000	0·041	0·000
*X*Jd	0·496	0·385	0·505	0·431	0·421	0·474	0·640	0·488	0·726
*X*Au	0·504	0·518	0·495	0·525	0·452	0·359	0·204	0·345	0·150
*X*Ac	0·000	0·097	0·000	0·045	0·097	0·129	0·155	0·127	0·124

*Total Fe as FeO.
†Total cations normalized to four for calculating ferric iron.
O.N., oxygen number.

than jadeitic-clinopyroxenite. On the other hand, the HREE and Y contents of clinopyroxenes in eclogite are slightly lower than those of counterparts in jadeitic-clinopyroxenite (Table 8 and Fig. 8). Clinopyroxene in eclogite has REE patterns that are convex-upward from La to Dy and concave-downward from Dy to Lu. Such HREE characteristics are only weakly developed in clinopyroxene from the jadeitic-clinopyroxenites. In particular, no HREE depletion is observed in jadeitic-clinopyroxenite MR47 that contains <0·1 vol. % of garnet. Clinopyroxenes in both eclogite and jadeitic-clinopyroxenite are poor in HFSE (Zr <1 ppm and

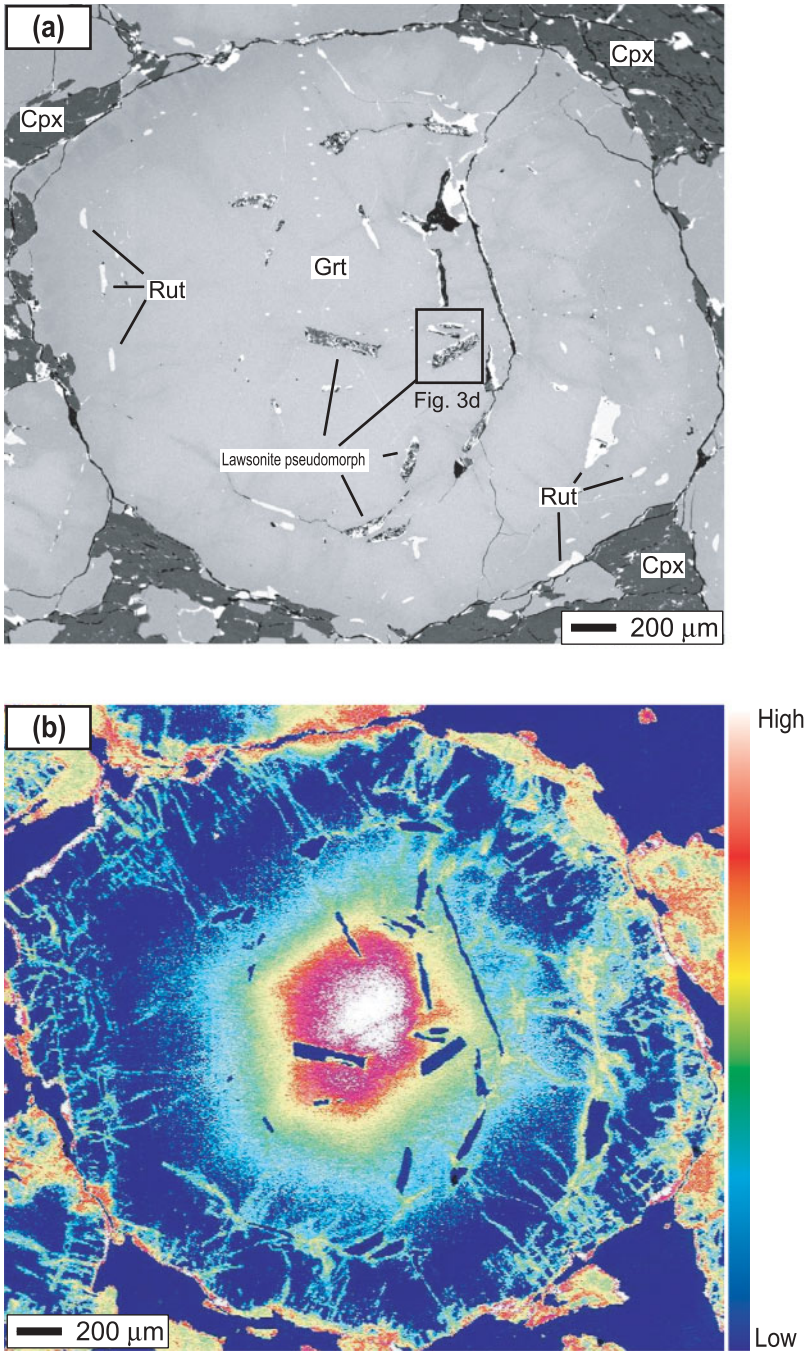

Fig. 5. (a) BSE image of garnet in jadeitic-clinopyroxenite MR3B. The garnet does not have any reaction rims. Lawsonite pseudomorphs preserve sharp and euhedral crystal boundaries of the original lawsonite, which are connected by cracks. (b) Electron microprobe X-ray map for Mn in the garnet shown in (a). White and red colors indicate higher concentration than green and blue.

Nb <0·001 ppm; Table 8). Other trace element data for clinopyroxene measured by ICP-MS are listed in Table 10.

Lawsonite and zoisite are rich in incompatible trace elements, especially U, Th, Pb, LREE and Sr. They are poor in high field strength elements (HFSE), similar to clinopyroxene (Tables 9 and 10). Matrix lawsonite from the lawsonite-eclogite sample has trace element abundances similar to those of matrix zoisite (Fig. 8e). The matrix lawsonites appear unzoned in trace elements, and the trace element abundances are almost identical among the matrix lawsonite grains in each sample.

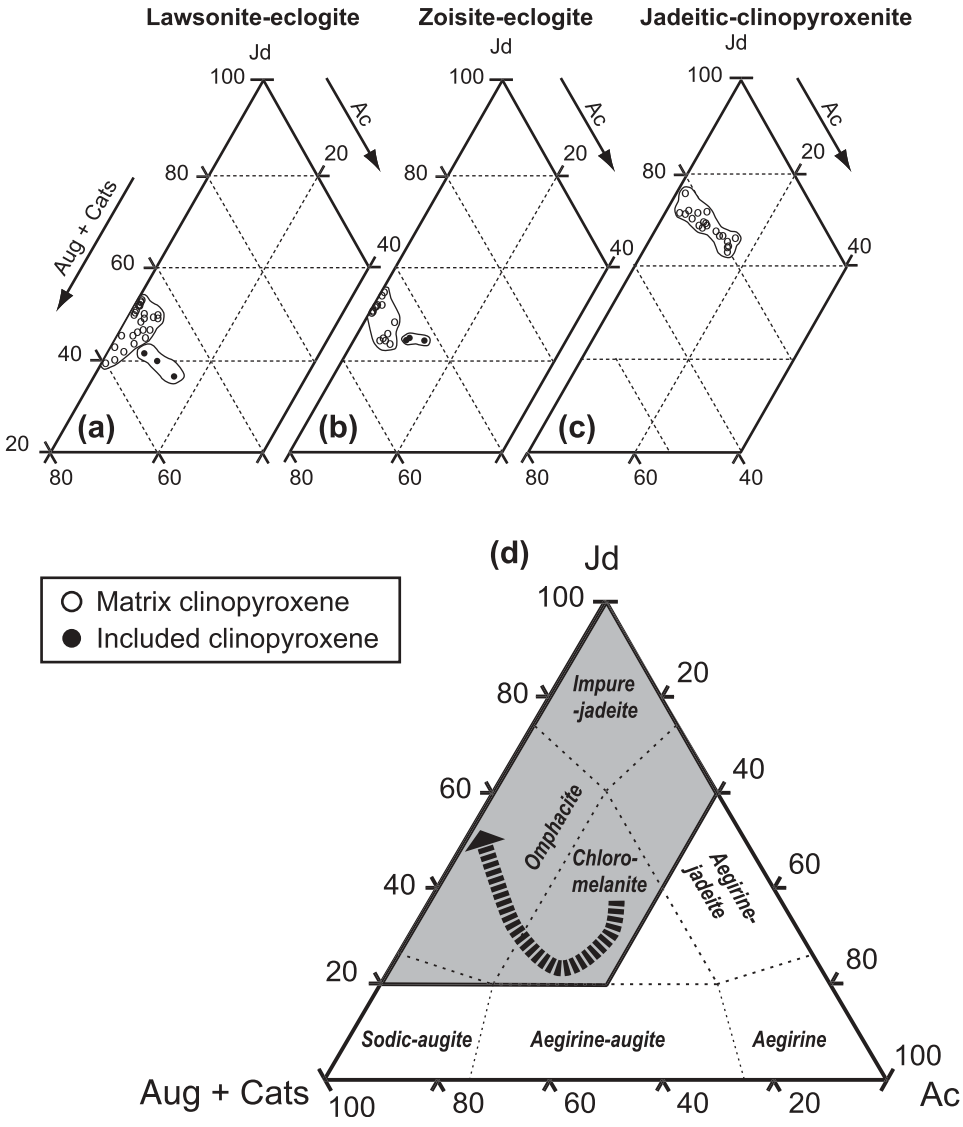

Fig. 6. Compositions of clinopyroxene in (a) lawsonite-eclogite GR1, (b) zoisite-eclogites, MR4 and MR7, and (c) jadeitic-clinopyroxenite MR3B plotted in the system Jd–Ac–(Aug + Cats). The shaded part of the full compositional triangle (d) is enlarged in (a), (b) and (c). Broken arrow in (d) shows the compositional change of clinopyroxene in basic rocks from the Franciscan metamorphic suite with increasing metamorphic pressure and temperature through to blueschist facies (Maruyama & Liou, 1988). The classification and the nomenclature of clinopyroxene follow Essene & Fyfe (1967).

However, matrix and included lawsonites display different REE patterns. Matrix lawsonites exhibit gently convex-upward LREE-enriched patterns from La to Er and relatively unfractionated patterns from Er to Lu. Included lawsonite grains have fairly flat REE patterns that decease slightly from La to Lu (Fig. 8). The trace element patterns of zoisite grains in eclogite and jadeitic-clinopyroxenite vary from sample to sample. For example, zoisite from apatite-bearing zoisite-eclogite MR7 contains less LREE than other zoisites (Fig. 8). This may reflect equilibration with apatite that is REE-rich (Usui, 2004). Other trace element data for zoisite measured by ICP-MS are listed in Table 10.

Whole-rock chemistry

Major element whole-rock compositions (Table 11) are plotted against SiO_2 contents in Fig. 10. Compositions of fresh and altered mid-ocean ridge basalt (MORB) from ocean-floor drilling holes 504B and 417D (Tual *et al.*, 1985; Zuleger *et al.*, 1995), and subduction-related metamorphic rocks thought to originate from MORB-type oceanic crust (Becker *et al.*, 1999; Bröcker & Enders, 2001; Gao & Klemd, 2001), are plotted for comparison.

Table 5: Representative electron microprobe analyses of lawsonite and zoisite

Mineral:	Lawsonite			Zoisite				
Rock type:	Lw-Ec		Zo-Ec	Lw-Ec	Zo-Ec		Jd-Cl	
Sample:	GR1		MR7	GR1	MR7	MR19	MR3B	MR26
Remarks:	matrix	inclusion	inclusion	matrix	matrix	matrix	inclusion	matrix
SiO_2	38·56	39·30	39·10	40·18	39·66	40·23	40·37	39·65
TiO_2	0·12	0·15	0·14	0·14	0·26	0·19	0·10	0·11
Al_2O_3	30·00	31·10	32·05	32·29	32·60	33·44	32·54	32·80
Cr_2O_3	0·19	0·25	0·19	0·19	0·04	0·06	0·15	0·07
Fe_2O_3	0·94	1·22	1·55	0·96	1·86	0·65	1·04	0·53
MnO	0·01	0·01	0·01	0·00	0·00	0·00	0·00	0·00
MgO	0·02	0·02	0·02	0·30	0·12	0·03	0·12	0·01
CaO	17·04	16·57	16·67	23·58	23·98	24·18	24·34	23·45
Na_2O	0·00	0·00	0·01	0·03	0·00	0·07	0·03	0·13
K_2O	0·00	0·00	0·00	0·00	0·04	0·01	0·01	0·01
NiO	0·00	0·00	0·00	0·00	0·09	0·01	0·00	0·00
Total	86·87	88·61	89·74	97·66	98·64	98·87	98·71	96·77
O.N.	8	8	8	12	12	12	12	12
Si	2·058	2·051	2·019	2·927	2·876	2·896	2·917	2·912
Ti	0·005	0·006	0·005	0·008	0·014	0·010	0·006	0·006
Al	1·887	1·913	1·950	2·773	2·787	2·837	2·771	2·839
Cr	0·008	0·010	0·008	0·011	0·002	0·003	0·008	0·004
Fe^{3+}	0·038	0·048	0·060	0·052	0·101	0·035	0·057	0·029
Mn	0·001	0·000	0·001	0·000	0·000	0·000	0·000	0·000
Mg	0·001	0·001	0·002	0·032	0·013	0·003	0·013	0·001
Ca	0·974	0·927	0·922	1·841	1·863	1·865	1·885	1·845
Na	0·000	0·000	0·001	0·004	0·000	0·010	0·004	0·018
K	0·000	0·000	0·000	0·000	0·004	0·001	0·001	0·001
Ni	0·000	0·000	0·000	0·000	0·005	0·001	0·000	0·000
Total	4·971	4·957	4·967	7·649	7·661	7·661	7·662	7·655

*Total Fe as Fe_2O_3.
O.N., oxygen number.

The whole-rock major element compositions of the eclogite and jadeitic-clinopyroxenite xenoliths do not lie in the ranges of either altered or fresh MORB. Instead, they are within the ranges of the subduction-related metamorphic rocks. In particular, the xenoliths are characterized by distinctively higher Na_2O contents with increasing SiO_2 contents than those of altered MORB, resulting in a continuous and near-linear trend on the SiO_2 vs Na_2O Harker diagram (Fig. 10b). In contrast, K_2O, FeO*, Al_2O_3, and TiO_2 in both eclogites and jadeitic-clinopyroxenites are almost identical to those of altered MORB. Such major element characteristics are commonly observed in metabasic rocks from subduction-related metamorphic terranes, and they have been explained by spilitization during high-temperature hydrothermal alteration at mid-ocean ridges and subduction-related metasomatism at fore-arc depths (e.g. Zack *et al.*, 2003). In particular, high Na_2O contents that are decoupled from K_2O contents are best explained by spilitization–albitization (Fig. 11). The jadeitic-clinopyroxenites are richer in Na_2O and SiO_2 than the eclogites, although there appears to be a continuous transition and overlap between the two groups. This reflects the differences in mineralogical composition and modal proportions of the major constituent minerals: Jd components in the clinopyroxenes are richer in the jadeitic-clinopyroxenites than those in the eclogites, and the jadeitic-clinopyroxenites contain more

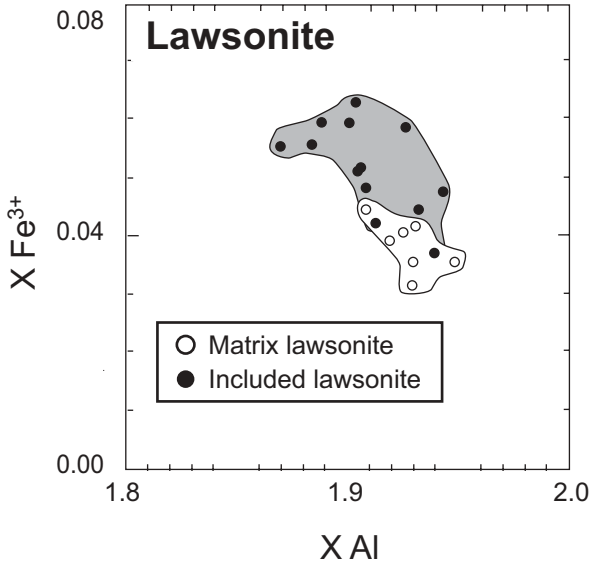

Fig. 7. $X\mathrm{Fe}^{3+}$ of lawsonite in lawsonite-eclogite GR1 plotted against $X\mathrm{Al}$. $X\mathrm{Fe}^{3+}$ and $X\mathrm{Al}$ are the cation numbers of Fe^{3+} and Al in lawsonite, respectively, when the oxygen number is eight.

clinopyroxene but less garnet, lawsonite and zoisite than the eclogites (compare Fig. 6 and Table 2 with Fig. 10).

Whole-rock chondrite-normalized REE patterns of eclogite and jadeitic-clinopyroxenite xenoliths are shown in Fig. 12; altered MORB from ocean-floor drilling hole 504B is shown as a shaded field for comparison. Eclogites have LREE-enriched patterns that decrease progressively from La to Lu, resulting in chondrite-normalized abundance ratios $[\mathrm{La/Lu}]_\mathrm{N} = 6{\cdot}0$–$11$ and $[\mathrm{La/Sm}]_\mathrm{N} = 2{\cdot}5$–$3{\cdot}3$ that are distinctively greater than those of altered MORB (Table 11). In addition to the higher abundance ratios, LREE concentrations are higher in the eclogite than in altered MORB. Jadeitic-clinopyroxenites display V-shaped REE patterns with the lowest normalized abundances at Eu. Although jadeitic-clinopyroxenites exhibit variable LREE contents, which are lower than those of the eclogites, their chondrite-normalized $[\mathrm{La/Sm}]_\mathrm{N}$ ratios are relatively constant and similar to those of the eclogite xenoliths. The REE patterns of eclogite and jadeitic-clinopyroxenite xenoliths are probably controlled by the modes of garnet and zoisite (or lawsonite), which have extremely different REE characteristics (Fig. 8). HFSE abundances are almost identical between eclogite and jadeitic-clinopyroxenite. The Zr/Hf and Nb/Ta ratios of the xenoliths vary from 36·9 to 37·6 and from 10·9 to 15·0, respectively. Both fall in the range of altered MORB, although the contents of these elements in the xenoliths are slightly higher than those of altered MORB (David *et al.*, 2000). The abundances of other trace elements, especially Pb, Sr and U, vary considerably; they are generally more abundant in eclogite than jadeitic-clinopyroxenite (Table 11).

Sr–Nd–Pb isotopic compositions

Whole-rock Sr, Nd and Pb isotopic data were age-corrected to 30 Ma (Table 12), the emplacement age of the host rock at Moses Rocks and Garnet Ridge (Naeser, 1971; Helmstaedt & Doig, 1975; Usui *et al.*, 2003), and are plotted on $^{87}\mathrm{Sr}/^{86}\mathrm{Sr}$–εNd, εNd–$^{206}\mathrm{Pb}/^{204}\mathrm{Pb}$, $^{206}\mathrm{Pb}/^{204}\mathrm{Pb}$–$^{207}\mathrm{Pb}/^{204}\mathrm{Pb}$ and $^{206}\mathrm{Pb}/^{204}\mathrm{Pb}$–$^{208}\mathrm{Pb}/^{204}\mathrm{Pb}$ diagrams (Fig. 13). The isotopic compositions of Juan de Fuca MORB and Phanerozoic Cordilleran crust, which represent Farallon MORB and its sedimentary cover, respectively, are shown for comparison.

The Sr isotopic ratios of the eclogites and jadeitic-clinopyroxenites vary ($^{87}\mathrm{Sr}/^{86}\mathrm{Sr} = 0{\cdot}7050$–$0{\cdot}7084$) and are greater than those of MORB. The jadeitic-clinopyroxenites have much higher Sr isotopic ratios than the eclogites. In contrast, the Nd isotopic compositions are similar in both eclogites and jadeitic-clinopyroxenites; εNd values vary from $-3{\cdot}1$ to $-1{\cdot}2$, much less than those of MORB, but similar to those of crustally derived sediments. Eclogites and jadeitic-clinopyroxenites have Pb isotopic compositions ($^{206}\mathrm{Pb}/^{204}\mathrm{Pb} = 18{\cdot}91$–$19{\cdot}38$, $^{207}\mathrm{Pb}/^{204}\mathrm{Pb} = 15{\cdot}62$–$15{\cdot}68$, and $^{206}\mathrm{Pb}/^{204}\mathrm{Pb} = 38{\cdot}68$–$38{\cdot}92$) that fall in the compositional field of sedimentary rocks in $^{206}\mathrm{Pb}/^{204}\mathrm{Pb}$–$^{207}\mathrm{Pb}/^{204}\mathrm{Pb}$ and $^{206}\mathrm{Pb}/^{204}\mathrm{Pb}$–$^{208}\mathrm{Pb}/^{204}\mathrm{Pb}$ diagrams (Fig. 13).

In addition to the whole-rock data, Rb–Sr, Sm–Nd and U–Th–Pb isotopic studies were also performed on garnet, clinopyroxene and zoisite mineral separates from the xenoliths (Table 13). The Pb isotopic compositions of garnet were not measured because of its extremely low Pb contents (0·038–0·087 ppm; see Table 10). Reference isochrons at 30 Ma were calculated to pass through each mineral in the $^{87}\mathrm{Sr}/^{86}\mathrm{Sr}$–$^{87}\mathrm{Rb}/^{86}\mathrm{Sr}$, $^{143}\mathrm{Nd}/^{144}\mathrm{Nd}$–$^{147}\mathrm{Sm}/^{144}\mathrm{Nd}$ and $^{206}\mathrm{Pb}/^{204}\mathrm{Pb}$–$^{238}\mathrm{U}/^{204}\mathrm{Pb}$ isotopic systems to distinguish isotopic equilibrium and disequilibrium at 30 Ma (Fig. 14). If one mineral was isotopically in equilibrium with another when the host diatremes were emplaced, the reference isochrons for the two minerals should be coincident within error. The slope of the reference isochron for the Rb–Sr system is almost horizontal because of the small variation of Rb/Sr ratio.

Figure 14a and b shows Rb–Sr isochron diagrams for representative eclogite sample MR19 and jadeitic-clinopyroxenite sample MR26; the diagrams include both mineral and whole-rock data. Both whole-rock values of $^{87}\mathrm{Sr}/^{86}\mathrm{Sr}$ are greater than those of the constituent minerals, although the minerals in the eclogite xenolith have almost identical Sr isotopic compositions. Individual minerals in the jadeitic-clinopyroxenite have different isotopic compositions, suggesting that they were not in equilibrium with each other at 30 Ma.

Table 6: Representative electron microprobe analyses of other constituent minerals

Mineral:	Phengite			Apatite			Orthoclase	Albite
Rock type:	Lw-Ec	Jd-Cl		Zo-Ec			Zo-Ec	Jd-Cl
Sample:	GR1	MR3B		MR7	MR7		MR7	MR26
Remarks:	matrix	matrix		matrix	matrix		inclusion	grain boundary
SiO_2	58·07	57·15	SiO_2	0·23	0·18	SiO_2	64·25	69·05
TiO_2	0·16	0·14	TiO_2	0·03	0·00	TiO_2	0·37	0·10
Al_2O_3	19·55	19·66	Al_2O_3	0·01	0·01	Al_2O_3	17·86	20·30
Cr_2O_3	0·06	0·07	Cr_2O_3	0·14	0·05	Cr_2O_3	0·00	2·50
FeO*	1·68	1·85	FeO*	0·00	1·15	Fe_2O_3†	1·45	0·00
MnO	0·00	0·01	MnO	0·33	0·00	MnO	0·00	0·00
MgO	7·16	6·63	MgO	0·14	0·00	MgO	0·00	0·07
CaO	0·01	0·00	CaO	54·88	55·50	CaO	0·08	10·11
Na_2O	0·04	0·05	Na_2O	0·00	0·00	Na_2O	0·00	0·09
K_2O	10·71	10·70	K_2O	0·01	0·00	K_2O	16·12	
NiO	0·00	0·00	P_2O_5	44·86	45·13	NiO		
Total	97·44	96·26	Total	100·63	102·00	Total	100·13	102·22
O.N.	22	22	O.N.	24	24	O.N.	8	8
Si	7·516	7·499	Si	0·035	0·027	Si	2·977	2·956
Ti	0·015	0·014	Ti	0·003	0·000	Ti	0·013	0·003
Al	2·983	3·040	Al	0·001	0·001	Al	0·976	1·024
Cr	0·006	0·008	Cr	0·017	0·005	Cr	0·000	
Fe^{2+}	0·182	0·203	Fe^{2+}	0·000	0·144	Fe^{3+}	0·050	0·081
Mn	0·000	0·001	Mn	0·043	0·000	Mn	0·000	0·000
Mg	1·382	1·298	Mg	0·032	0·000	Mg	0·000	0·000
Ca	0·001	0·000	Ca	8·930	8·949	Ca	0·004	0·003
Na	0·009	0·013	Na	0·000	0·000	Na	0·000	0·839
K	1·769	1·791	K	0·002	0·000	K	0·953	0·005
Ni	0·000	0·000	P	5·956	5·937	Ni		
Total	13·863	13·866	Total	15·020	15·064	Total	4·973	4·911

*Total Fe as FeO.
†Total Fe as Fe_2O_3.
O.N., oxygen number.

The reference Sm–Nd isochrons for all minerals and the whole-rock of eclogite are coincident within error (Fig. 14c), but garnet from the jadeitic-clinopyroxenite has a different Nd isotopic composition from the other minerals and the whole-rock (Fig. 14d). Zoisites display almost identical Sm/Nd abundance ratios and Nd isotopic compositions to those of the whole-rocks because they are the dominant reservoir for LREE in both eclogite and jadeitic-clinopyroxenite (as discussed later; see Fig. 15).

The Pb isotopic compositions of clinopyroxene in the eclogite xenoliths are almost in equilibrium with zoisite at 30 Ma (Fig. 14e). In contrast, the Pb isotopic compositions of clinopyroxene and zoisite in jadeitic-clinopyroxenite are not in equilibrium with each other at 30 Ma. Such features are weakly observed in the other U-series isochron diagrams ($^{207}Pb/^{204}Pb$–$^{235}U/^{204}Pb$ and $^{208}Pb/^{204}Pb$–$^{232}Th/^{204}Pb$). Although zoisite is the dominant host of U and Pb, it has distinctively different Pb isotopic compositions and U/Pb abundance ratios from those of the whole-rocks. This might be explained by the presence of zircons with extremely high $^{238}U/^{204}Pb$ ($>10^6$) and $^{206}Pb/^{204}Pb$ ($>10^3$) (Usui, 2004).

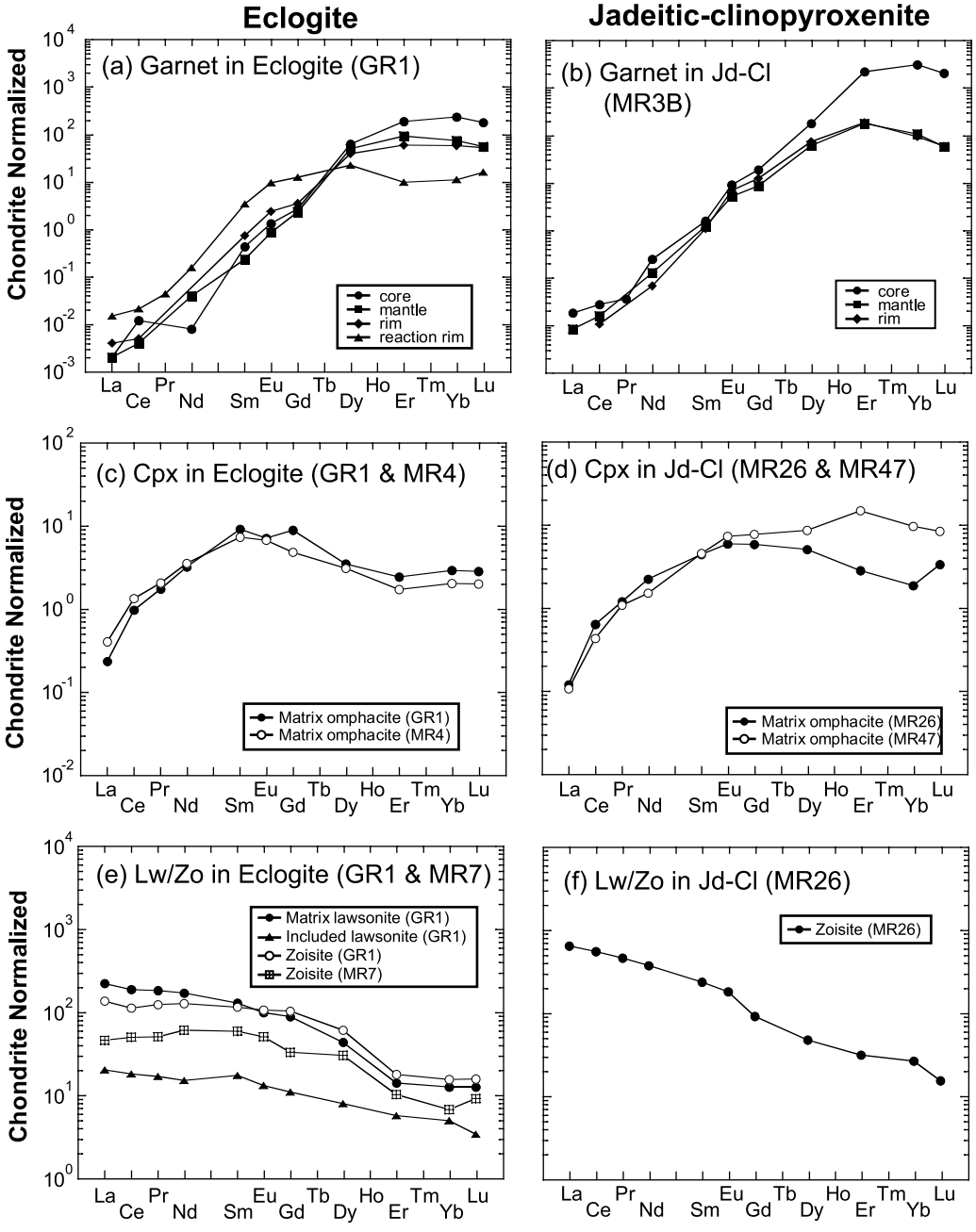

Fig. 8. Chondrite-normalized rare earth element patterns of garnet, clinopyroxene, lawsonite and zoisite in eclogites (GR1, MR4 and MR7) and jadeitic-clinopyroxenites (M26 and MR47). The rare earth element data are normalized to the C1 chondrite value of Sun & McDonough (1989).

DISCUSSION

Evidence for high-*P*/*T* prograde metamorphism

The compositional zoning structure of garnet and the inclusion assemblages within garnet grains in eclogites and jadeitic-clinopyroxenites preserve information about a certain range of the *P*–*T* history of the xenoliths. The Sps component of garnet in both xenolith types is markedly zoned and preserves a fine euhedral structure (Fig. 5). Mn zoning of this type is not observed in other mantle-derived eclogite xenoliths; however, it is common in garnet-bearing regional metamorphic rocks that have undergone prograde metamorphism (e.g. Atherton & Edmunds, 1966; Zack *et al.*, 2004). The Mn zoning of the garnet in the xenoliths is thus interpreted to reflect growth during prograde metamorphism.

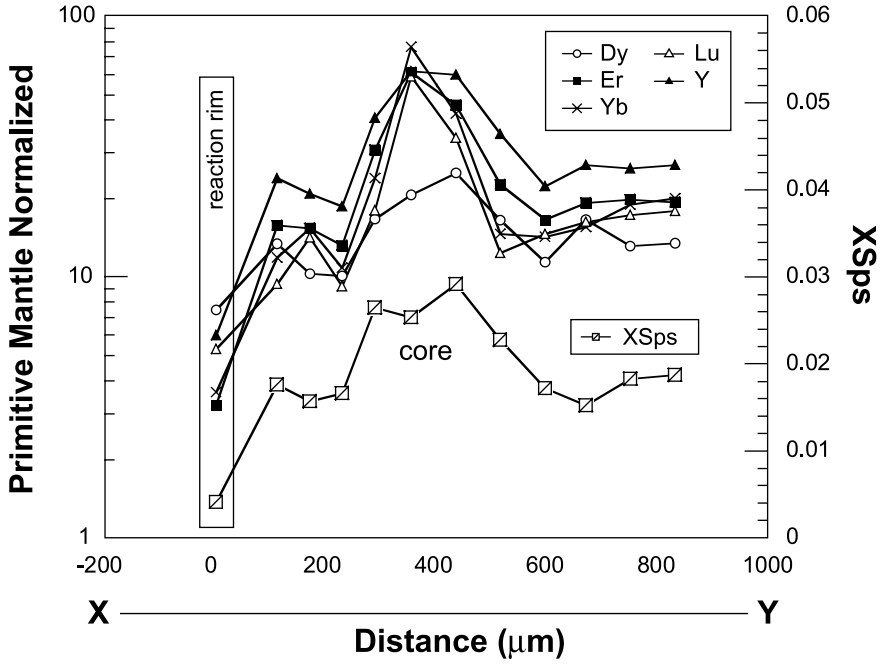

Fig. 9. Zoning profiles along traverse X–Y in Fig. 2a for HREE, Y and Mn (*X*Sps) in the garnet. Concentrations of Dy, Er, Yb, Lu and Y were analyzed simultaneously by ion microprobe, and are normalized to the primitive mantle value of Sun & McDonough (1989). The Mn content of the garnet next to the ion microprobe pits was analyzed by electron microprobe.

Included clinopyroxenes are richer in Ac and poorer in Jd contents than matrix clinopyroxene (Fig. 6). This probably reflects jadeite–acmite substitution. Clinopyroxene generally becomes more jadeitic and less acmitic with increasing pressure and temperature in the upper blueschist to eclogite facies (Maruyama & Liou, 1988). Most included lawsonite grains have higher Fe_2O_3 and lower Al_2O_3 contents than matrix lawsonite (Fig. 7). Maruyama & Liu (1988) reported negative correlations between Fe^{3+} and Al molar abundances in lawsonite during progressive metamorphism at blueschist facies: Fe^{3+} content decreases with increasing pressure and temperature. Thus, included clinopyroxene and lawsonite probably formed in a lower pressure and temperature metamorphic environment than matrix clinopyroxene and lawsonite.

Garnet grains from the Colorado Plateau eclogites contain curved trails of fine-grained coesite and rutile inclusions (Fig. 2d), indicating the former presence of a planar tectonic fabric (see also Helmstaedt & Schulze, 1988, 1991). Such textures do not commonly form by magmatic processes, but are commonly found in regional metamorphic suites, such as those of Corsica and the Franciscan metamorphic complex of the western USA, which are known for their occurrences of high-pressure and low-temperature eclogites (Caron & Pèquignot, 1986; Maruyama & Liou, 1988). Thus, the inclusions indicate that the immediate protolith of the eclogite xenoliths was a fine-grained foliated rock, probably a blueschist.

In summary, garnet crystals grew during prograde metamorphism, and successively captured minerals such as clinopyroxene and lawsonite, reaching peak metamorphic conditions ranging from 560 to 700°C at 3 GPa and to 600 to 760°C at 5 GPa (Usui *et al.*, 2003). Such high-*P*–low-*T* environments, which are colder than typical mantle geotherms, can be achieved only in subducted oceanic lithosphere. Therefore, we propose that the Colorado Plateau eclogite xenoliths formed by prograde metamorphic recrystallization of subducted oceanic crust.

'Retrogression' of eclogite xenoliths during emplacement

The Colorado Plateau eclogites were entrained within and rapidly transported to the surface by the host ultramafic microbreccia diatremes during the Tertiary (~30 Ma). The eclogite xenoliths exhibit less retrograde overprinting than subduction-related eclogites from high-pressure metamorphic terranes, as indicated by the absence of amphibole. However, some modifications resulting from xenolith–host-rock interaction are observed. In the lawsonite-eclogite xenoliths, the lawsonite grains are invariably rimmed by zoisite, and, in the zoisite-eclogite xenoliths, the lawsonite is totally replaced

Table 7: Representative ion microprobe trace element analyses of garnet (ppm)

Mineral:	Garnet										
Rock type:	Lw-Ec				Zo-Ec						
Sample:	GR1				MR7			MR4			
Remarks:	core	mantle	rim	reaction rim	core	mantle	reaction rim	core	mantle	rim	reaction rim
Sr	0·063	0·066	0·051	0·039	0·22	0·091	0·083	0·68	0·12	0·12	0·12
Y	281	186	119	27	402	193	132	1007	358	120	18
Zr	0·24	0·14	0·21	3·5	0·39	0·17	0·38	33	0·44	0·20	6·7
Nb	0·001	0·001	0·001	0·001	0·001	n.d.	0·001	0·70	0·001	0·001	n.d.
La	0·001	n.d.	0·001	0·003	0·002	0·001	0·006	0·020	0·002	0·003	0·002
Ce	0·007	0·002	0·003	0·01	n.d.	0·002	0·013	0·027	0·003	0·005	0·004
Pr	n.d.	n.d.	n.d.	0·004	n.d.	n.d.	0·001	0·012	0·000	n.d.	n.d.
Nd	0·004	0·018	0·000	0·070	0·011	0·004	0·062	0·054	0·019	0·015	0·011
Sm	0·064	0·035	0·11	0·50	0·029	0·008	0·25	0·14	0·14	0·062	0·19
Eu	0·074	0·048	0·13	0·53	0·081	0·039	0·20	0·16	0·20	0·085	0·24
Gd	0·54	0·46	0·69	2·5	0·58	0·39	1·8	1·3	1·6	0·65	1·0
Dy	15	12	9·7	5·5	19	8·1	14	38	30	8·9	3·0
Er	29	15	9·5	1·6	66	29	6·9	123	35	9·4	0·93
Yb	38	12	9·4	1·8	200	61	4·0	297	33	12	0·85
Lu	4·4	1·3	1·3	0·39	34	10	0·55	38	3·9	1·4	0·18

Mineral:	Garnet					
Rock type:	Jd-Cl					
Sample:	MR3B			MR26		
Remarks:	core	mantle	rim	core	mantle	rim
Sr	0·19	0·079	0·053	0·41	0·16	0·27
Y	330	199	56	879	728	126
Zr	12	2·9	1·2	0·47	0·32	0·35
Nb	0·001	n.d.	0·001	0·001	n.d.	n.d.
La	0·004	0·001	n.d.	0·004	0·002	0·002
Ce	0·001	0·002	0·003	0·016	0·015	0·009
Pr	0·002	0·004	0·004	0·003	n.d.	n.d.
Nd	0·085	0·25	0·14	0·11	0·16	0·056
Sm	0·69	2·3	1·8	0·22	0·39	0·17
Eu	0·31	0·84	0·72	0·49	1·5	0·28
Gd	5·9	12	6·6	3·6	9·5	1·6
Dy	39	28	9·4	42	109	14
Er	31	13	3·9	336	158	27
Yb	33	17	4·2	474	45	16
Lu	5·5	2·9	0·70	48	3·8	1·4

n.d., not detected.

Table 8: Representative ion microprobe trace element analyses of clinopyroxene (ppm)

Mineral:	Clinopyroxene					
Rock type:	Lw- Ec		Zo-Ec	Jd-Cl		
Sample:	GR1	GR1	MR4	MR3B	MR26	MR47
Remarks:	matrix	inclusion	matrix	matrix	matrix	matrix
Sr	21	21	49	9·3	17	4·3
Y	4·4	3·7	3·6	9·5	3·8	11
Zr	0·66	0·63	0·71	0·58	0·49	2·2
Nb	0·001	0·001	0·001	n.d.	n.d.	0·003
La	0·056	0·046	0·11	0·030	0·029	0·026
Ce	0·50	0·060	0·97	0·21	0·40	0·27
Pr	0·15	0·013	0·24	0·084	0·11	0·10
Nd	1·5	0·15	2·3	0·85	1·0	0·71
Sm	1·1	0·16	1·4	0·90	0·67	0·69
Eu	0·39	0·037	0·52	0·39	0·34	0·42
Gd	1·8	0·18	1·6	1·7	1·2	1·6
Dy	1·509	0·71	1·1	2·3	1·3	2·2
Er	0·41	0·69	0·25	1·5	0·46	2·4
Yb	0·49	0·44	0·42	1·1	0·31	1·6
Lu	0·099	0·055	0·075	0·17	0·084	0·21

n.d., not detected.

Table 9: Representative ion microprobe analyses of trace elements in lawsonite and zoisite (ppm)

Mineral:	Lawsonite	Zoisite				
Rock type:	Lw-Ec	Lw-Ec	Zo-Ec		Jd-Cl	
Sample:	GR1	GR1	MR7	MR4	MR3B	MR26
Remarks:	matrix	matrix	matrix	matrix	inclusion	matrix
Sr	897	768	511	22574	397	2278
Y	26	43	28	1·2	319	28
Zr	0·048	0·16	0·094	0·25	2·2	0·13
Nb	0·010	0·009	0·007	0·37	0·006	0·015
La	51	32	11	116	26	147
Ce	103	66	30	190	109	310
Pr	14	11	4·6	28	21	40
Nd	70	56	27	120	133	156
Sm	18	17	8·5	29	72	31
Eu	5·0	5·8	2·8	25	7·8	9·8
Gd	15	20	6·3	126	58	17
Dy	9·6	14	7·3	3·5	92	12
Er	1·9	2·8	1·6	0·47	44	5·4
Yb	2·2	2·4	1·0	1·7	39	4·1
Lu	0·31	0·38	0·22	0·24	4·9	0·40

n.d., not detected.

by zoisite. Although similar replacement reactions of lawsonite are commonly observed in lawsonite-bearing eclogites from regional metamorphic belts (e.g. Zack *et al.*, 2004), the mineral products and their textures in the regional metamorphic eclogites are different from those in the Colorado Plateau eclogite xenoliths. Whereas lawsonite pseudomorphs in the Colorado Plateau eclogite xenoliths contain only fibrous and radiating zoisite aggregates, those in regional metamorphic eclogites are replaced by well-crystallized multiple mineral phases, such as epidote, paragonite, phengite and albite (Zack *et al.*, 2004). Because lawsonite is stable at lower-T and higher-P conditions than these replacing minerals (e.g. Schmidt & Poli, 1998; Poli & Schmidt, 2002), breakdown of lawsonite could occur as a result of increasing temperature and/or decreasing pressure during a retrogression event. The petrographical difference in lawsonite pseudomorphs between the Colorado Plateau eclogite xenoliths and regional metamorphic eclogites may reflect the nature of the P–T path of retrograde metamorphism. The radiating and fibrous textures of zoisite and preservation of lawsonite in the Colorado Plateau eclogite xenoliths suggest that the zoisite crystallized rapidly by replacement of lawsonite under disequilibrium conditions, probably during the transport of the lawsonite-eclogites in the host rocks.

The textures and major element compositions of zoisite are almost identical in both lawsonite- and zoisite-eclogite xenoliths (Figs 2 and 3 and Table 5). Moreover, zoisite-eclogite xenoliths lack matrix lawsonite but contain included lawsonite in unfractured garnet (Fig. 3c). Thus, the textural and mineralogical differences between the lawsonite- and zoisite-eclogites could reflect varying extents of recrystallization induced by the host rock. Both types of eclogite xenoliths could, therefore, have been originally lawsonite-eclogites.

Garnet compositions are almost uniform within individual mineral grains, except for variations in the Mg/Fe ratio in some reaction rims (Figs 2a and 5). Such rims display extremely pyrope-rich compositions relative to other parts of the garnet, suggesting that they crystallized at higher temperature conditions than the rest of the grain. The reaction rims are well developed in zoisite-rich eclogite. Moreover, the pyrope-rich compositions are also observed along cracks within the garnet grains that connect to lawsonite pseudomorphs (Fig. 3b). On the other hand, such reaction rims are not found in jadeitic-clinopyroxenite xenoliths, which have little or no

Table 10: Trace element compositions of separated minerals measured by ICP-MS

Mineral:	Garnet			Clinopyroxene			Zoisite		
Rock type:	Zo-Ec	Zo-Ec	Jd-Cl	Zo-Ec	Zo-Ec	Zo-Ec	Zo-Ec	Zo-Ec	Jd-Cl
Sample:	MR15	MR19	MR26	MR15	MR19	MR26	MR15	MR19	MR26
$\mu g/g$									
Rb	0·033	0·049	0·13	0·044	0·049	0·084	4·3	8·3	5·1
Sr	3·4	3·9	4·4	34	16	24	6210	2965	4214
Y	103	66	156	3·0	4·1	2·4	21	33	27
Zr	—	—	—	—	—	—	—	—	—
Nb	—	—	—	—	—	—	—	—	—
Cs	0·0007	0·0012	0·0015	0·0010	0·0009	0·0030	0·26	0·45	0·29
Ba	0·60	0·52	3·8	0·45	1·1	4·0	72	106	198
La	0·023	0·27	0·13	0·19	1·4	0·16	190	254	174
Ce	0·074	0·51	0·28	0·54	3·2	0·49	375	529	360
Pr	0·015	0·076	0·04	0·13	0·48	0·10	41	64	44
Nd	0·17	0·36	0·20	0·81	2·4	0·63	167	277	186
Sm	0·59	0·41	0·42	1·0	1·2	0·35	38	72	57
Eu	0·57	0·31	0·46	0·17	0·25	0·13	7·9	14	9·8
Gd	3·6	2·4	3·7	0·67	1·0	0·54	23	43	31
Tb	1·5	0·9	1·8	0·14	0·17	0·10	2·4	4·2	3·6
Dy	13	8·0	18	0·75	0·91	0·61	7·4	12	12
Ho	2·9	2·2	4·8	0·12	0·17	0·11	0·75	1·2	1·2
Er	7·9	6·2	14	0·21	0·40	0·26	1·0	1·6	1·3
Tm	1·2	1·0	2·2	0·030	0·059	0·036	0·11	0·091	0·090
Yb	8·4	7·1	15·3	0·17	0·40	0·24	0·42	0·52	0·49
Lu	1·2	1·0	2·2	0·019	0·052	0·031	0·051	0·086	0·048
Hf	—	—	—	—	—		—	—	—
Pb	0·038	0·070	0·087	0·34	0·28	0·35	48	51	68
Th	0·030	0·067	0·090	0·074	0·45	0·11	28	37	32
U	0·037	0·038	0·12	0·027	0·11	0·029	8·0	5·8	5·3

zoisite aggregate after lawsonite. Formation of the reaction rim was probably related to the alteration of lawsonite to zoisite, which liberated fluid that catalyzed the reaction.

Heterogeneous trace element distributions in the subducted oceanic crust

Colorado Plateau eclogite xenoliths have been interpreted to represent fragments of the subducted Farallon plate (probably altered oceanic crust) that underwent high-*P*/*T* metamorphism in the lawsonite eclogite facies (Usui *et al.*, 2003). Therefore, the compositions of the xenoliths should carry a record of the trace element characteristics of the subducted oceanic crust in the Farallon plate. In this study, we have determined element distributions of Rb, Sr, Sm, Nd, U, Th and Pb between the constituent minerals, garnet, clinopyroxene and zoisite. Rb–Sr, Sm–Nd and U–Pb isotopic systematics of both constituent minerals and whole-rocks allows the degree of isotopic equilibrium and disequilibrium to be evaluated.

Mass balance calculations were performed by comparing the measured whole-rock data with calculated whole-rock data. The calculated whole-rock data were obtained by multiplying density-weighted modal abundances of the constituent minerals by their trace element concentrations, and summing each mineral's contribution. The ICP-MS analyses for separated minerals were used as average values for the trace element contents of each mineral (Table 10). Differences between measured and calculated whole-rock compositions may point to undetected accessory phases. The calculations also indicate the dominant carriers of each trace

Table 11: Major and trace element compositions of whole-rock samples

Rock type:	Zo-Ec				Jd-Cl			
Sample:	MR15	MR19	MR49	MR29	MR26	MR21	MR50	MR47
wt %								
SiO_2	51·19	52·01	53·41	48·96	51·79	52·33	53·16	55·91
TiO_2	0·78	1·35	0·97	1·50	1·45	1·16	1·21	1·11
Al_2O_3	15·39	16·53	17·77	16·38	16·45	17·55	14·39	17·21
Fe_2O_3*	7·24	8·94	7·03	9·36	10·24	9·22	8·93	6·46
MnO	0·14	0·16	0·12	0·16	0·18	0·18	0·18	0·12
MgO	7·20	5·40	3·83	7·63	5·24	4·69	5·32	2·93
CaO	9·95	7·24	5·34	9·77	7·04	5·99	6·33	3·60
Na_2O	6·23	7·78	9·75	4·96	7·64	8·21	9·09	11·92
K_2O	0·051	0·097	0·12	0·145	0·082	0·21	0·11	0·038
P_2O_5	0·001	0·006	0·000	0·002	0·003	0·000	0·003	0·001
LOI	1·31	0·42	1·06	0·77	0·12	0·77	0·46	0·97
Total	99·52	99·97	99·43	99·68	100·25	100·34	99·22	100·30
ppm								
Cr_2O_3	132	258	164	298	219	265	251	125
NiO	147	103	71	182	90	105	158	85
ppm								
Li	67	52	85	38	65	63	66	102
Rb[1]	0·880	2·12	3·03	1·46	2·35	3·34	2·51	1·95
Sr[1]	582	281	447	574	207	387	82·8	30·6
Y	20	25	13	25	30	42	25	8·8
Zr	169	194	168	119	163	177	146	153
Nb	6·3	9·9	8·6	8·4	8·9	10	8·0	10·7
Cs	0·071	0·67	0·46	0·19	0·73	0·96	0·077	0·55
Ba	69	92	686	108	470	65	222	25
La	22	33	13	17	3·7	9·3	2·7	2·6
Ce	42	67	22	33	8·0	21	5·7	5·6
Pr	5·0	8·5	2·8	4·0	1·0	2·6	0·83	0·82
Nd[1]	18·7	37·4	10·7	18·8	4·50	10·1	4·32	2·52
Sm[1]	4·03	7·92	2·45	4·74	1·20	2·38	1·50	0·796
Eu	1·2	1·8	0·8	1·5	0·41	0·74	0·47	0·27
Gd	4·0	6·0	2·3	4·7	1·8	3·1	2·3	1·2
Tb	0·65	0·75	0·35	0·67	0·48	0·68	0·52	0·23
Dy	3·6	4·0	2·0	3·8	4·0	5·6	3·8	1·5
Ho	0·66	0·82	0·42	0·79	1·0	1·4	0·90	0·34
Er	1·6	2·2	1·2	2·0	2·9	4·1	2·5	0·93
Tm	0·24	0·34	0·19	0·31	0·46	0·67	0·42	0·15
Yb	1·6	2·3	1·4	2·1	3·3	4·8	2·9	1·1
Lu	0·22	0·34	0·21	0·31	0·48	0·69	0·41	0·15
Hf	4·5	5·2	4·5	3·2	4·4	4·7	4·0	4·1
Ta	0·58	0·78	0·69	0·62	0·59	0·76	0·61	0·73
Pb[1]	5·6	3·2	4·2	5·1	1·8	2·3	0·63	0·17
Th[1]	2·7	5·6	1·8	2·0	0·93	2·8	1·6	1·1
U[1]	1·3	1·9	0·99	1·1	0·67	0·93	0·75	0·49
Zr/Hf	37·2	37·3	37·5	37·4	36·9	37·6	37·0	37·1
Nb/Ta	10·9	12·6	12·5	13·5	15·0	13·2	13·2	14·7
$[La/Sm]_N$	3·29	3·01	3·32	2·47	2·01	2·32	1·24	1·78
$[La/Lu]_N$	11·0	10·6	6·71	6·03	0·833	1·45	0·702	1·82

*Total Fe given as Fe_2O_3.
[1]Rb, Sr, Sm, Nd, U, Th and Pb concentrations were measured by the ID-TIMS method.
LOI, loss on ignition.

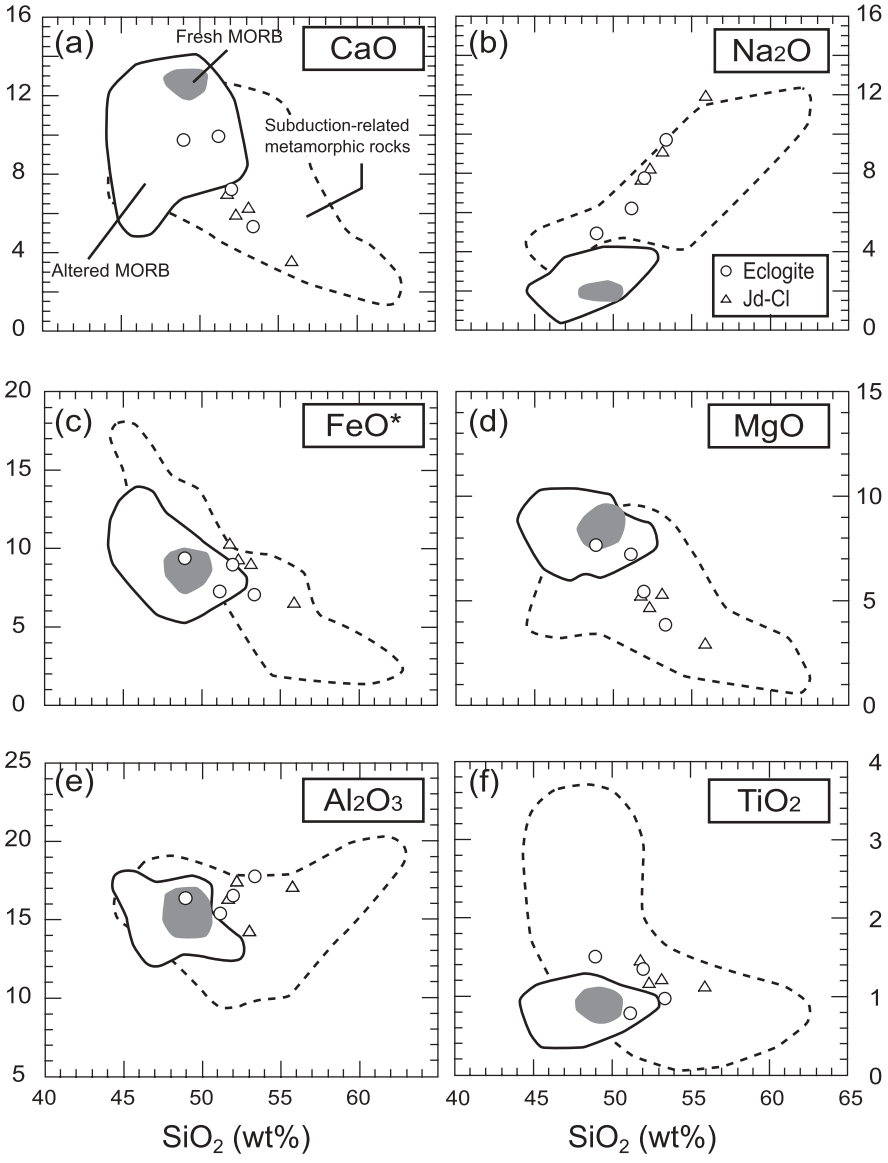

Fig. 10. Whole-rock major element compositions (wt % oxide) of the eclogite and jadeitic-clinopyroxenite xenoliths as a function of SiO_2 content (wt %). ○, eclogite; △, jadeitic-clinopyroxenite. Compositional fields of fresh MORB and altered MORB are based on data from Tual *et al.* (1985) and Zuleger *et al.* (1995), and that of subduction-related metamorphic rocks, which represent MORB-type oceanic crust, is from Becker *et al.* (1999), Bröcker & Enders (2001) and Gao & Klemd (2001).

element. Figure 15 shows the results of the calculations for zoisite-eclogite MR19 and jadeitic-clinopyroxenite xenolith MR26.

Mass balance can be achieved only for HREE; garnet controls the HREE and Y budgets of the whole-rock. Although zoisite hosts the other REE (especially LREE), Sr, Th and Pb, the calculated whole-rock compositions of these elements are more than twice as much as those of the measured whole-rock compositions. These overestimates of calculated compositions against measured compositions might be caused by overestimates of the modal proportions of zoisite. For modal proportion determinations by optical microscope, areas of lawsonite pseudomorphs that were totally replaced by zoisite aggregates were defined as zoisite. Because fine-grained and radiating zoisite aggregates cannot be completely embedded in the lawsonite pseudomorphs owing to their morphology (Figs 2 and 3), the modal proportion of zoisite is likely to be overestimated. The obvious deficits of Cs, Rb and Ba can be explained by the lack of analyses of phengite for Cs, Rb and Ba, and barite for Ba. These deficits are observed in the jadeitic-clinopyroxenite (Fig. 15). Barite could have been formed by surface weathering after exhumation of the xenoliths

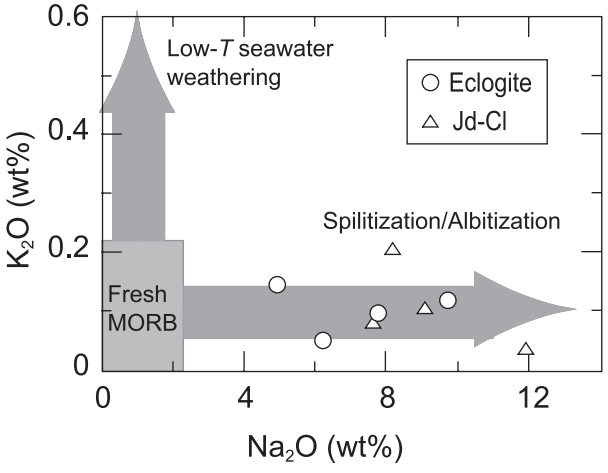

Fig. 11. Whole-rock Na_2O and K_2O contents (wt %) in eclogite and jadeitic-clinopyroxenite xenoliths. The field of fresh MORB (data sources as in Fig. 10) and trends produced by spilitization–albitization and low-*T* seawater alteration (see text for explanation) are also shown.

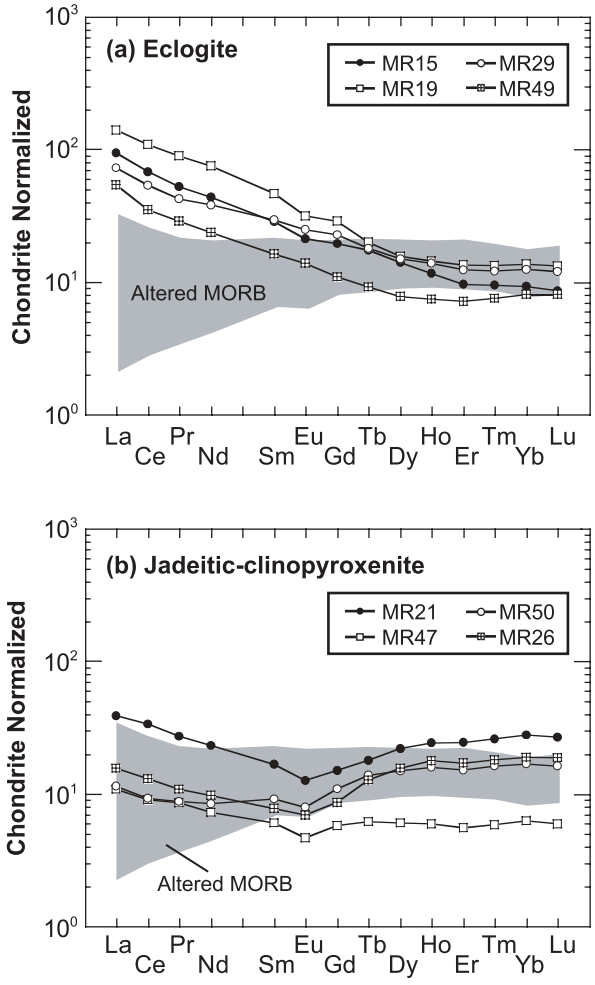

Fig. 12. Whole-rock rare earth element patterns of (a) eclogite and (b) jadeitic-clinopyroxenite xenoliths normalized to the C1 chondrite values of Sun & McDonough (1989). Shaded area shows the compositional field of altered MORB after Bach *et al.* (2003).

to the surface by the host-rock emplacement, because it has not been found as part of the primary mineral assemblage of the eclogites and occurs only as fine-grained crystals along the grain boundaries of the other primary minerals, such as garnet and clinopyroxene. The deficit for U cannot be explained and might be attributed to the presence of an unknown U-enriched phase.

Our results for trace element distributions in the Colorado Plateau eclogite xenoliths are generally consistent with previous studies regarding eclogite samples from regional metamorphic belts (Tribuzio *et al.*, 1996; Zack *et al.*, 2002*a*, 2002*b*; Spandler *et al.*, 2003). In some regional metamorphic eclogites and garnet-amphibolites, allanite dominates the whole-rock REE, U and Th budgets, instead of lawsonite and zoisite (Sorensen & Grossman, 1989, 1993; Tribuzio *et al.*, 1996). This reflects the difference in metamorphic pressure and temperature conditions between these regional metamorphic eclogites and the Colorado Plateau eclogite xenoliths. The regional metamorphic eclogites underwent lower-*P* and/or higher-*T* metamorphic conditions than our xenoliths, in which neither lawsonite nor zoisite was stable.

We tested for isotopic equilibrium among the constituent minerals by examining the Rb–Sr, Sm–Nd and U–Th–Pb systematics of both minerals and whole-rocks. The mass balance calculations suggest that, except for U, these elements are concentrated almost exclusively in the zoisite that crystallized during xenolith emplacement (Fig. 15). This means that zoisite and the whole-rock should plot close together in the isochron diagrams or, if this is not the case, another phase with extremely different isotopic compositions and element ratios, not accounted for in the mass balance, must be suspected in the rocks. The former case was observed in the Sm–Nd isochron diagram, and the latter in both the Rb–Sr and U–Pb diagrams.

As seen in the Rb–Sr isochron diagrams (Fig. 14a and b), the whole-rock $^{87}Sr/^{86}Sr$ isotopic ratios are distinctly higher than those of zoisite. This discrepancy could be explained by the presence of barite crystals, which contain abundant Sr (up to 20 wt % as Sr oxide). Differences in $^{87}Sr/^{86}Sr$ between whole-rock and zoisite are much larger in the jadeitic-clinopyroxenite. This may reflect differences in the contributions of barite to the whole-rock Sr budget between eclogite and jadeitic-clinopyroxenite, because eclogite contains more zoisite, which dominates the whole-rock Sr, than jadeitic-clinopyroxenite.

Table 12: Sr, Nd and Pb isotopic compositions of whole-rock samples

Rock type:	Zo-Ec				Jd-Cl			
Sample:	MR15	MR19	MR49	MR29	MR26	MR21	MR50	MR47
Rb	0·880	2·12	3·03	1·46	2·35	3·34	2·51	1·95
Sr	582	281	447	574	207	387	82·8	30·6
$^{87}Sr/^{86}Sr$ (measured)	0·705277	0·706492	0·706001	0·705016	0·707147	0·708420	0·708257	0·707571
2σ	0·000009	0·000009	0·000008	0·000008	0·000008	0·000008	0·000007	0·000010
$^{87}Rb/^{86}Sr$	0·00437	0·0218	0·0197	0·0073	0·0329	0·0249	0·0879	0·184
$^{87}Sr/^{86}Sr$ (30 Ma)*	0·705275	0·706482	0·705993	0·705013	0·707133	0·708409	0·708220	0·707492
Sm	4·03	7·92	2·45	4·74	1·20	2·38	1·50	0·796
Nd	18·7	37·4	10·7	18·8	4·50	10·1	4·32	2·52
$^{143}Nd/^{144}Nd$ (measured)	0·512480	0·512561	0·512533	0·512559	0·512540	0·512512	0·512480	0·512572
2σ	0·000008	0·000007	0·000007	0·000007	0·000006	0·000007	0·000007	0·000006
$^{147}Sm/^{144}Nd$	0·130073	0·127951	0·138749	0·152086	0·160553	0·142611	0·209680	0·190964
εNd (30 Ma)*†	−2·8	−1·2	−1·8	−1·4	−1·8	−2·3	−3·1	−1·3
U	1·30	1·86	0·993	1·05	0·667	0·931	0·751	0·489
Th	2·72	5·64	1·81	2·02	0·933	2·83	1·62	1·06
Pb	5·60	3·17	4·24	5·06	1·80	2·27	0·628	0·171
$^{206}Pb/^{204}Pb$ (measured)‡	19·327	19·150	19·044	18·979	19·152	19·268	19·741	20·164
$^{207}Pb/^{204}Pb$ (measured)‡	15·679	15·646	15·628	15·626	15·647	15·666	15·697	15·679
$^{208}Pb/^{204}Pb$ (measured)‡	38·855	38·921	38·724	38·728	38·873	39·042	39·013	39·351
$^{238}U/^{204}Pb$	15·0	38·0	15·0	13·3	23·9	26·6	77·9	189
$^{235}U/^{204}Pb$	0·109	0·275	0·109	0·0968	0·173	0·193	0·565	1·37
$^{232}Th/^{204}Pb$	32·4	118·7	28·4	26·5	34·6	83·5	174	421
$^{206}Pb/^{204}Pb$ (30 Ma)*	19·257	18·973	18·974	18·917	19·041	19·144	19·377	19·285
$^{207}Pb/^{204}Pb$ (30 Ma)*	15·676	15·638	15·625	15·623	15·642	15·660	15·680	15·638
$^{208}Pb/^{204}Pb$ (30 Ma)*	38·807	38·744	38·682	38·689	38·821	38·918	38·755	38·726

*Isotopic compositions at 30 Ma.
†εNd values were calculated relative to CHUR $^{143}Nd/^{144}Nd = 0·512638$ and $^{147}Sm/^{144}Nd = 0·1967$ (Wasserburg *et al.*, 1981).
‡Analytical errors for Pb isotopic ratios followed reproducibility obtained by repeated analyses of JB3 (see Table A1).

For the ^{238}U–^{206}Pb isochron diagrams, the whole-rocks of both zoisite-eclogite and jadeitic-clinopyroxenite plot far from the zoisites and their reference isochrons (Fig. 14e and f). This discrepancy is explained by the presence of young zircons (33–81 Ma) with high $^{238}U/^{204}Pb$ ($>10^6$) and $^{206}Pb/^{204}Pb$ ($>10^3$) ratios (Usui, 2004). Although these zircons should also affect the whole-rock data for ^{235}U–^{207}Pb and ^{232}Th–^{208}Pb systematics, their isotopic signatures are not clearly observed in the ^{235}U–^{207}Pb and ^{232}Th–^{208}Pb isochron diagrams, because the natural abundance ratio of $^{235}U/^{238}U$ is low (1/137·88) and contents of Th are lower than those of U.

The zoisite-eclogite xenolith MR19 consists of garnet, clinopyroxene and zoisite that equilibrated at 30 Ma, the age of emplacement of the host diatreme, although the Sr isotopic composition of the zoisite is slightly higher than those of the other minerals (Fig. 14a, c and e). The mineral isochron ages for zoisite-eclogite xenoliths are 39 ± 11 Ma for the $^{147}Sm/^{144}Nd$–$^{143}Nd/^{144}Nd$ isochron diagram, and 33 ± 20 Ma for the $^{238}U/^{206}Pb$–$^{207}Pb/^{206}Pb$ isochron diagram. Despite large errors, both of the mineral isochron ages are consistent with the U–Pb ages of zircons in the zoisite-eclogites (Usui *et al.*, 2003), and with the emplacement ages of the host diatremes (Naeser, 1971; Helmstaedt & Doig, 1975; Roden *et al.*, 1979). On the other hand, it is difficult to obtain meaningful isotopic ages from the $^{87}Rb/^{86}Sr$–$^{87}Sr/^{86}Sr$, $^{147}Sm/^{144}Nd$–$^{143}Nd/^{144}Nd$ and $^{238}U/^{206}Pb$–$^{207}Pb/^{206}Pb$ isochron diagrams for jadeitic-clinopyroxenite xenolith MR26 (Fig. 14b, d and f). If clinopyroxene and garnet in MR26 were isotopically homogenized, the pair should yield identical isochron ages among the different isotopic systems. However, this is not the case, and the

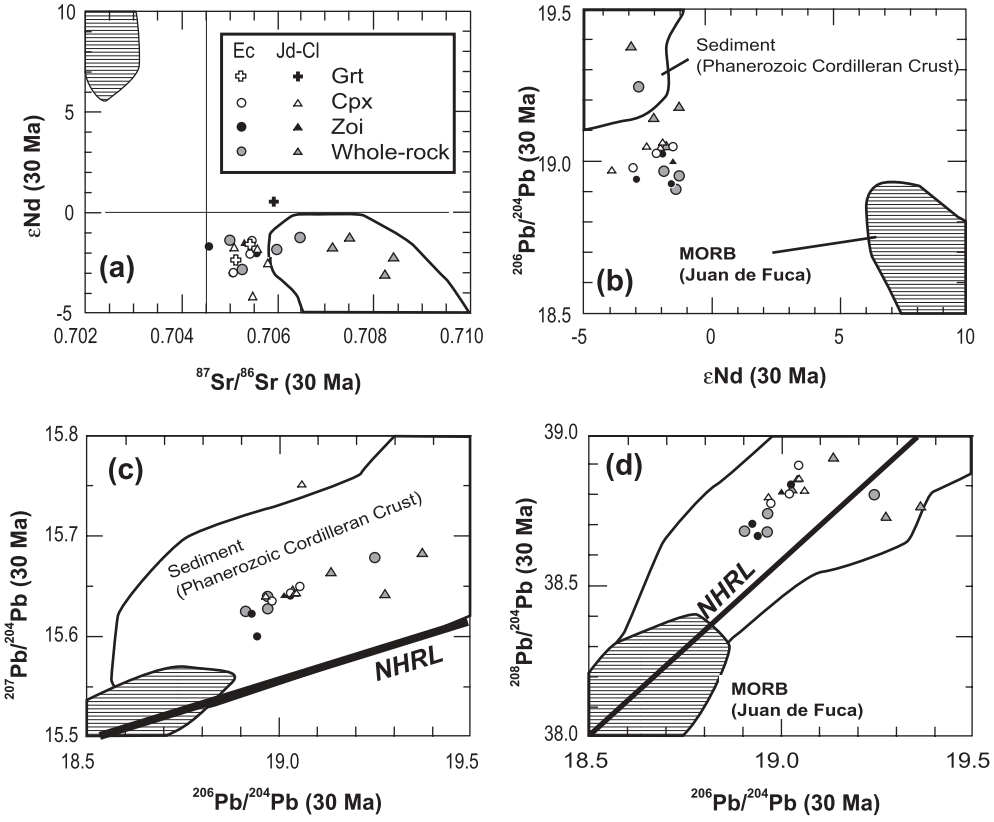

Fig. 13. Sr–Nd–Pb isotopic compositions of whole-rocks and the constituent minerals in eclogite and jadeitic-clinopyroxenite xenoliths plotted in (a) εNd vs $^{87}Sr/^{86}Sr$, (b) $^{206}Pb/^{204}Pb$ vs εNd, (c) $^{207}Pb/^{204}Pb$ vs $^{206}Pb/^{204}Pb$, and (d) $^{208}Pb/^{204}Pb$ vs $^{206}Pb/^{204}Pb$ diagrams. All measured data were age-corrected to 30 Ma. Compositional fields of Juan de Fuca MORB and Phanerozoic Cordilleran crust are based on data from Church & Tatsumoto (1975), Aleinikoff (1987), Hegner & Tatsumoto (1987), White *et al.* (1987) and Farmer *et al.* (1993). Northern Hemisphere Reference Line (NHRL; Hart, 1984) is also shown.

ages obtained for $^{87}Rb/^{86}Sr$–$^{87}Sr/^{86}Sr$ and for $^{147}Sm/^{144}Nd$–$^{143}Nd/^{144}Nd$ are 492 ± 27 Ma and 42·4 ± 6·7 Ma, respectively. Moreover, mineral isochron ages obtained for zoisite combined with garnet and clinopyroxene are geologically unreasonable (for example, the zoisite–clinopyroxene mineral isochron age in the $^{87}Rb/^{86}Sr$–$^{87}Sr/^{86}Sr$ system is 13 400 ± 700 Ma).

The differences in mineral isochron ages between the zoisite-eclogite and the jadeitic-clinopyroxenite are related to the amount of fluid that was generated by lawsonite breakdown to zoisite aggregates during diatreme emplacement. Fluid not only catalyzes metamorphic reactions, but it also facilitates rapid mass transport. In the zoisite-eclogite xenoliths, the availability of fluids evidently allowed the recrystallization of zircons, which yield U–Pb concordia ages almost identical to those of microbreccia intrusion (Usui *et al.*, 2003). Because the zoisite-eclogite contains abundant zoisite aggregates that were originally lawsonite, isotopic homogenization was probably facilitated by the presence of fluids, which evidently induced recrystallization of parts of garnet and clinopyroxene and caused diffusive isotopic resetting preferentially along cracks and grain boundaries. Petrographic observations indicate that almandine-rich garnet in the zoisite-eclogites recrystallized pyrope-rich compositions not only at the rim, but also along cracks into the garnet cores (Fig. 3b). Thus, all the mineral isochron ages and the U–Pb zircon ages in the zoisite-eclogite represent the emplacement age of the microbreccia diatreme.

In contrast, the jadeitic-clinopyroxenites contain little or no zoisite, reflecting a lawsonite-poor precursor. This lack of prograde lawsonite resulted in little or no fluid production during retrogression associated with the microbreccia emplacement. The experimentally determined volume diffusion rates for Pb and Nd in clinopyroxene (Sneeringer *et al.*, 1984; van Orman *et al.*, 1998; Cherniak, 2001) are too slow to have changed the isotopic ratios during diatreme emplacement without a fluid phase. In the absence of fluids, minerals have been shown to preserve their isotopic signatures far above their commonly accepted closure temperatures, even for time scales of entire orogenic metamorphic episodes (Farquhar *et al.*, 1996; Tilton *et al.*, 1997; Kelley &

Table 13: Sr, Nd and Pb isotopic compositions of minerals

Mineral:	Clinopyroxene						
Rock type:	Zo-Ec			Jd-Cl			
Sample:	MR15	MR19	MR29	MR26	MR21	MR50	MR47
Rb	0·00625	0·0135	0·250	0·0301	0·292		0·0371
Sr	39·7	18·8	51·7	22·1	18·8		7·37
$^{87}Sr/^{86}Sr$ (measured)	0·705096	0·705436	0·705490	0·705588	0·705826		0·705105
2σ	0·000011	0·000016	0·000009	0·000013	0·000008		0·000010
$^{87}Rb/^{86}Sr$	0·00045	0·00208	0·01400	0·00393	0·04509		0·01457
$^{87}Sr/^{86}Sr$ (30 Ma)*	0·705095	0·705435	0·705484	0·705586	0·705807		0·705099
Sm	0·494	0·904	0·286	0·353	0·807		0·597
Nd	0·853	2·49	0·576	0·611	1·43		1·28
$^{143}Nd/^{144}Nd$ (measured)	0·5125112	0·5125326	0·5125822	0·5125649	0·5125352		0·5125555
2σ	0·0000050	0·0000044	0·0000073	0·0000056	0·0000084		0·0000065
$^{147}Sm/^{144}Nd$	0·350	0·219	0·301	0·349	0·341		0·282
εNd (30 Ma)*†	−3·1	−2·1	−1·5	−2·0	−2·6		−1·9
U	0·462	0·336	0·703	0·361	0·259	0·258	0·0531
Th	0·136	0·338	0·0637	0·128	0·280	0·702	0·353
Pb	0·0412	0·0495	0·0516	0·0262	0·0760	0·0957	0·0460
$^{206}Pb/^{204}Pb$ (measured)‡	19·007	19·073	19·074	19·065	19·137	19·082	19·327
$^{207}Pb/^{204}Pb$ (measured)‡	15·635	15·643	15·649	15·645	15·648	15·646	15·765
$^{208}Pb/^{204}Pb$ (measured)‡	38·803	38·904	38·908	38·892	38·967	39·070	39·488
$^{238}U/^{204}Pb$	5·73	9·51	4·73	4·67	18·9	24·0	56·6
$^{235}U/^{204}Pb$	0·0415	0·0690	0·0343	0·0339	0·137	0·174	0·410
$^{232}Th/^{204}Pb$	19·6	67·2	6·04	23·6	72·1	182	449
$^{206}Pb/^{204}Pb$ (30 Ma)*	18·980	19·029	19·052	19·044	19·049	18·970	19·063
$^{207}Pb/^{204}Pb$ (30 Ma)*	15·634	15·641	15·648	15·644	15·644	15·641	15·752
$^{208}Pb/^{204}Pb$ (30 Ma)*	38·774	38·804	38·899	38·857	38·860	38·799	38·821

Mineral	Zoisite				Garnet		
Rock type	Zo-Ec			Jd-Cl	Zo-Ec		Jd-Cl
Sample	MR15	MR19	MR29	MR26	MR15	MR19	MR26
Rb	3·24	5·89	1·96	3·36	0·00457	0·103	0·0681
Sr	5035	2567	5487	3634	3·22	11·6	3·79
$^{87}Sr/^{86}Sr$ (measured)	0·705022	0·705523	0·704526	0·705324	0·705142	0·705443	0·705924
2σ	0·000009	0·000011	0·000011	0·000011	0·000008	0·000008	0·000009
$^{87}Rb/^{86}Sr$	0·00186	0·00664	0·00103	0·00268	0·00410	0·0255	0·0519
$^{87}Sr/^{86}Sr$ (30 Ma)*	0·705021	0·705521	0·704526	0·705323	0·705141	0·705432	0·705902
Sm	31·3	54·1	45·6	36·7	0·624	0·975	0·402
Nd	156	249	191	171	0·165	1·16	0·152
$^{143}Nd/^{144}Nd$ (measured)	0·5124707	0·5125242	0·5125449	0·5125444	0·5129242	0·5126173	0·5129361
2σ	0·0000057	0·0000065	0·0000041	0·0000076	0·0000199	0·0000060	0·0000082
$^{147}Sm/^{144}Nd$	0·121	0·131	0·145	0·130	2·29	0·509	1·596
εNd (30 Ma)*†	−3·0	−2·0	−1·6	−1·6	−2·4	−1·6	0·5

Table 13: Continued

Mineral	Zoisite				Garnet		
Rock type	Zo-Ec			Jd-Cl	Zo-Ec		Jd-Cl
Sample	MR15	MR19	MR29	MR26	MR15	MR19	MR26
U	47·7	43·8	40·4	63·5			
Th	27·2	34·8	18·6	28·7			
Pb	7·30	5·37	2·98	4·84			
$^{206}Pb/^{204}Pb$ (measured)‡	18·989	19·065	18·950	19·032			
$^{207}Pb/^{204}Pb$ (measured)‡	15·602	15·642	15·624	15·641			
$^{208}Pb/^{204}Pb$ (measured)‡	38·721	38·911	38·750	38·862			
$^{238}U/^{204}Pb$	9·82	7·91	4·73	4·91			
$^{235}U/^{204}Pb$	0·0713	0·0574	0·0343	0·0356			
$^{232}Th/^{204}Pb$	37·9	52·9	30·5	30·1			
$^{206}Pb/^{204}Pb$ (30 Ma)*	18·943	19·028	18·928	19·009			
$^{207}Pb/^{204}Pb$ (30 Ma)*	15·600	15·641	15·623	15·640			
$^{208}Pb/^{204}Pb$ (30 Ma)*	38·665	38·832	38·704	38·818			

*Isotopic compositions at 30 Ma.
†εNd values were calculated relative to CHUR $^{143}Nd/^{144}Nd = 0{\cdot}512638$ and $^{147}Sm/^{144}Nd = 0{\cdot}1967$ (Wasserburg *et al.*, 1981).
‡Analytical errors for Pb isotopic ratios followed reproducibility obtained by repeated analyses of JB3 (see Table A1).

Wartho, 2000). Therefore, the constituent minerals in the jadeitic-clinopyroxenite xenoliths were probably not in equilibrium, and their mineral isochron ages are, thus, meaningless. Fortunately, however, the isotopic compositions of these minerals allow us to infer the pristine isotopic compositions of subducted oceanic crust prior to isotopic homogenization by diatreme emplacement.

Infiltration of metasomatizing fluids derived from sedimentary rocks

Although the chemical compositions of lithologies likely to be subducted (i.e. variably altered oceanic crust and overlying sedimentary cover) have been well investigated by ocean-floor drilling (e.g. Alt, 1995), chemical characterization of the subducted lithologies remains relatively poorly studied. In particular, there are few reliable datasets for the Sr, Nd and Pb isotopic compositions of subducted materials (e.g. Bernard-Griffiths & Cornichet, 1985; Thöni & Jagoutz, 1992; Becker *et al.*, 2000). Such data could be used to constrain whole-mantle and individual subduction-zone chemical recycling models, and to explain the enriched isotopic signatures of OIB and island arc magmas (e.g. Hofmann, 1997; Shibata & Nakamura, 1997; Taylor & Nesbitt, 1998; van Keken *et al.*, 2002). In this section, we discuss the isotopic and trace element compositions of the subducted materials, based on the geochemical datasets obtained from the Colorado Plateau eclogite xenoliths.

Both the eclogite and jadeitic-clinopyroxenite xenoliths from the Colorado Plateau, which are interpreted to represent subducted oceanic crust, exhibit 'geochemically enriched' Sr, Nd and Pb isotopic compositions and whole-rock trace element patterns (Figs 12 and 13). Because the whole-rock trace element abundances of the xenoliths are likely to have been modified by hydrothermal alteration at the mid-ocean ridge, where the MORB protolith formed, and by metasomatism during subduction (Becker *et al.*, 1999, 2000), they cannot be used to constrain their protoliths, e.g. normal-type MORB (N-MORB) or enriched-MORB (E-MORB). In addition, we cannot discount the possibility that the xenoliths represent fragments of OIB, similar to Hawaiian tholeiites and associated subalkaline rocks, which probably occurred sporadically on the Farallon plate. However, the eclogite and the jadeitic-clinopyroxenite xenoliths have almost constant Zr/Hf ratios ranging from 36·9 to 37·6 (Table 11). Such values are consistent with all types of MORB, but not with OIB (David *et al.*, 2000). The MORB-like Zr/Hf ratios of the xenoliths are evidence against a seamount origin, because Zr and Hf are relatively immobile elements, and the Zr/Hf ratios should not change during subduction. Even if any of the different MORB-types are protoliths for the xenoliths, their Sr, Nd and Pb isotopic signatures

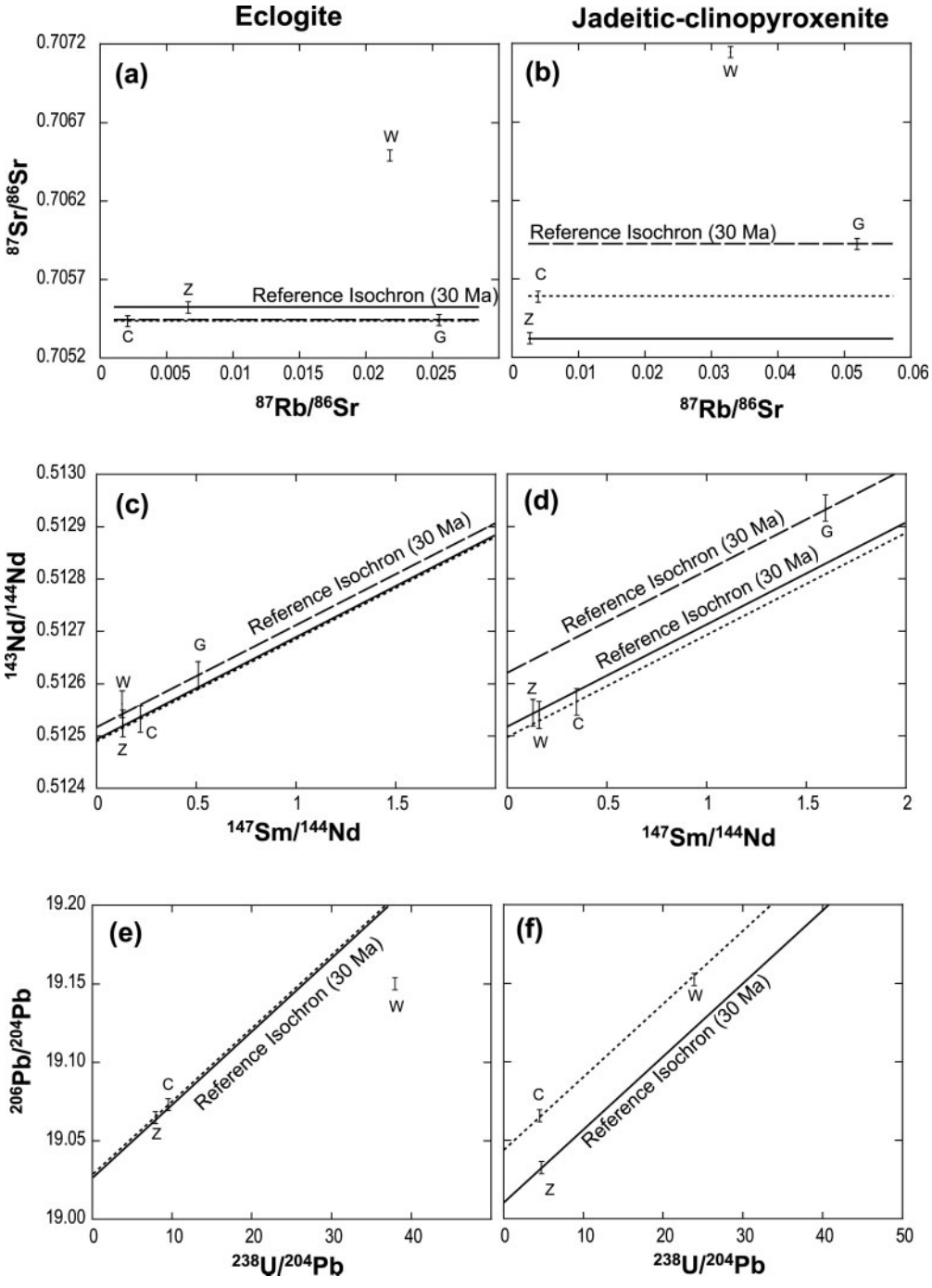

Fig. 14. Rb–Sr, Sm–Nd and U–Pb isochron diagrams for constituent minerals in eclogite MR19 (a, c, and e) and jadeitic-clinopyroxenite MR26 (b, d and f) xenoliths. The lines marked in each figure are 30 Ma reference isochrons, which were calculated to pass through the three constituent minerals: G, garnet; C, clinopyroxene; Z, zoisite; W, whole-rock. Continuous line, zoisite; dotted line, clinopyroxene; dashed line, garnet. Vertical bar shows standard deviation (2σ) in Table A1.

reflect the addition of an enriched geochemical component to the xenoliths.

The Sr, Nd and Pb isotopic compositions of the constituent minerals of the Colorado Plateau eclogite xenoliths are used to identify the source of the enriched component, because the whole-rock isotopic data were probably contaminated by surface weathering and/or interaction with the microbreccia host rock. A surface weathering effect is seen in the difference between the Sr isotopic compositions of the whole-rocks and those of

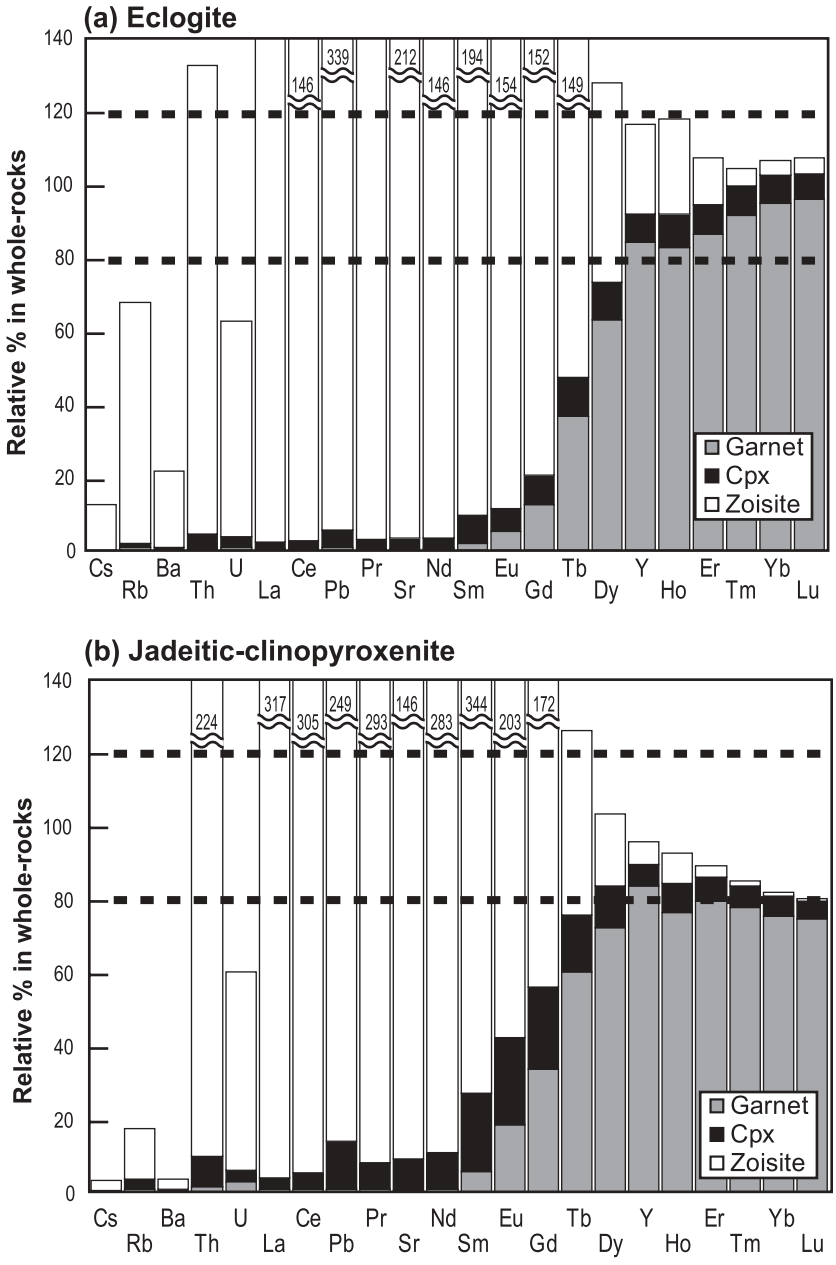

Fig. 15. Mass balance calculations for (a) eclogite MR19 and (b) jadeitic-clinopyroxenite MR26. Density-weighted modal abundances of minerals are calculated by multiplying the mode in vol. % in Table 2 by densities. The densities are interpolated from values of Deer *et al.* (1992): 4·1 for $Alm_{70}Pyr_{30}$ garnet; 3·3 for omphacitic clinopyroxene; 3·15 for zoisite. Bar length corresponds to the amount of the trace element in each phase in relative proportion to the whole-rock concentration. If the total amount of the relative proportions of the minerals falls in the range 80–120%, mass balances are judged to be achieved, considering uncertainties in modal proportions of minerals and heterogeneity in their trace element concentrations; outside this range, either the uptake of trace elements in an unanalyzed phase or overestimation of modal proportions is suspected.

the constituent minerals (Fig. 13a) and is best explained by the presence of late barite along grain boundaries. Differences in Pb isotopic compositions between whole-rocks and minerals were also observed (e.g. Fig. 13c). If abundant geochemical components originating in the microbreccia transport medium were added to the xenoliths, the mineral isotopic compositions of the eclogite xenoliths would be unusable, because, in contrast to the jadeitic-clinopyroxenite xenoliths, the eclogite minerals reached isotopic equilibrium during diatreme emplacement. However, judging from the REE element patterns of garnet and clinopyroxene (Fig. 8), such mag-

matic influences on the geochemistry of the constituent minerals of the xenoliths were probably small. Therefore, the mineral isotopic signatures observed not only the jadeitic-clinopyroxenite but also in the eclogite xenolith could represent the Sr, Nd and Pb isotopic compositions of the subducted basaltic oceanic crust.

The Sr, Nd and Pb isotopic compositions of the constituent minerals in the xenoliths are thought to reflect mixing between an 'altered MORB component' and a 'sedimentary component', based on considerations of the possible lithologies subducted with the protolith of the xenoliths in the Farallon plate (Fig. 13). The isotopic variations could have resulted from combining heterogeneous sedimentary components with variably altered MORB in variable mixing ratios. Such mixing cannot be explained by mechanical mixing between metasedimentary rocks and altered MORB crust, because a mechanical mixing model is inconsistent with the basaltic bulk-rock major element composition of the xenoliths. Instead, it requires metasomatic alteration induced by migration of a fluid from sedimentary layers to the basaltic protolith. Because the quantity of fluids and fluid mobility are limited in high-grade metamorphic conditions (e.g. Scambelluri & Philippot, 2001) metasomatism probably occurred at an early stage of subduction. At shallow levels (<10 km depth), large volumes of predominantly sedimentary rock and detritus accumulate in accretionary wedges, occurring in many subduction complexes as mélange-like material between the slab and the hanging wall (Shreve & Cloos, 1986). Such subduction mélanges contain mafic and ultramafic blocks showing varying extents of metasomatic alteration as a result of infiltrating aqueous fluids (Sorensen, 1988; Sorensen & Grossman, 1989, 1993). Although the Colorado Plateau eclogite xenoliths might not have been derived from mafic blocks in a mélange unit, studies of mélanges yield insights into the metasomatic mixing process. Detailed isotopic studies of a subduction mélange unit (Bebout, 1991) have suggested that large amounts of aqueous fluid, previously equilibrated with metasedimentary rocks, enter the mafic–ultramafic mélange, and produce large-scale stable isotopic homogenization and pervasive metasomatism. Therefore, in the fore-arc region, the protolith of the eclogite and jadeitic-clinopyroxenite xenoliths could have been metasomatized by large volumes of fluid derived from associated metasedimentary units.

Reassessment of Precambrian model ages

The Colorado Plateau eclogite xenoliths have distinctively lower εNd values than MORB at any time in the Phanerozoic (Roden *et al.*, 1990; Wendlandt *et al.*, 1993; this study). Wendlandt *et al.* (1993) applied Sm–Nd isotope systematics to determine the age of oceanic lithosphere that could have contributed to the protolith of the Colorado Plateau eclogite xenoliths. The Nd isotopic compositions and Sm/Nd ratios of the xenolith samples were used to calculate the time at which the xenolith would have the εNd value of the depleted mantle evolution curve proposed by DePaolo *et al.* (1991). However, the Nd isotopic compositions as well as the Sm/Nd ratios of MORB can be modified by subduction-related metasomatic events after extraction of the MORB melts from the depleted mantle at a mid-ocean ridge (e.g. Jahn *et al.*, 1996). As discussed above, the Colorado Plateau eclogite xenoliths were metasomatized by large amounts of fluid that were isotopically equilibrated with metasedimentary rocks. To obtain accurate Nd model ages, Wendlandt *et al.* (1993) selected 'less' altered eclogite xenoliths based on their whole-rock chemistries. Nevertheless, these eclogite xenoliths have weak V-shaped REE patterns and distinctively higher $[La/Sm]_N$ ratios (0·97–1·29) than those of MORB, suggesting that even they have undergone metasomatism. Thus, Nd model ages are an unsatisfactory measure of the protolith age for the Colorado Plateau eclogite xenoliths.

Smith *et al.* (2004) reported Proterozoic U–Pb zircon ages from the Colorado Plateau eclogite xenoliths. Nine multigrain zircon fractions were analyzed with TIMS following the chemical separation of Pb and U. Four of the nine multigrain zircon fractions almost plot on the concordia growth curve and yield ages from 35 to 70 Ma, consistent with the age range reported by Usui *et al.* (2003). The other five multigrain zircon fractions were discordant. Smith *et al.* (2004) selected seven multigrain zircon fractions from the nine fractions, and then obtained a poorly fit discordia (MSWD = 92) between 34·9 ± 3·3 and 1514 ± 74 Ma. The discordant zircon fractions were interpreted to establish that Colorado Plateau eclogites contained inherited mid-Proterozoic zircons. From this Smith *et al.* (2004) concluded that the Colorado Plateau eclogites represent fragments of Proterozoic lithosphere, and that the concordant young ages between 35 and 70 Ma record episodic zircon growth as a result of Mesozoic or Cenozoic eclogite-facies recrystallization of Proterozoic mantle. However, the reliability of the Proterozoic discordant U–Pb age must be further investigated, because all discordant multigrain zircon fractions plot close to the lower intercept (<10% of concordance from the upper intercept). The Smith *et al.* (2004) model is also inconsistent with the euhedral zoning structure of Mn in garnet and the garnet inclusion assemblages described in this paper. These petrographic features are incompatible with the postulated eclogite-facies recrystallization processes in the upper mantle but are better explained by subduction-related prograde metamorphism.

CONCLUSIONS

Eclogite and jadeitic-clinopyroxenite xenoliths from the Colorado Plateau consist of garnet, clinopyroxene, lawsonite and zoisite with minor amounts of phengite, rutile, pyrite and zircon. The xenoliths have basaltic whole-rock major element compositions, but significantly higher Na_2O with increasing SiO_2 contents compared with those of altered MORB. These major element characteristics are interpreted to reflect spilitization during hydrothermal alteration in a mid-ocean ridge environment, followed by subduction-related metasomatism in the fore-arc. Euhedral garnet zoning structures and the major element compositions of included clinopyroxene and lawsonite indicate that the xenoliths underwent subduction-related prograde metamorphism. Fine-grained zoisite aggregates crystallized rapidly, formed by replacement of lawsonite during the transport of lawsonite-eclogite to the surface in the microbreccia host. These petrographic results are consistent with those of Usui *et al.* (2003), who proposed that the Colorado Plateau eclogite xenoliths originated as fragments of subducted oceanic crust comprising part of the Farallon plate, which has resided in the upper mantle since the Late Cretaceous.

The whole-rock chemistry of the xenoliths has variable trace element enrichment compared with MORB or altered MORB, except for the Zr/Hf ratio, which ranges from 36·9 to 37·6. Whole-rock mass balance analysis demonstrates the trace element distributions among the constituent minerals in the xenoliths. Garnet is the principal residence site for HREE and Y, and zoisite hosts the other REE (especially LREE), Sr, Th and Pb. In the eclogite xenoliths, garnet, clinopyroxene and zoisite were in approximate isotopic equilibrium at the time of emplacement (~30 Ma). These minerals yield ^{147}Sm–^{143}Nd mineral isochron ages of 39 ± 11 Ma and ^{238}U–^{206}Pb ages of 33 ± 20 Ma. In contrast, the same minerals in the jadeitic-clinopyroxenite xenoliths were not in isotopic equilibrium at the time of diatreme emplacement. The fluid released by the breakdown of lawsonite during the entrainment by the microbreccia host may have facilitated isotopic equilibration in the eclogite xenoliths.

Based on the Sr–Nd–Pb isotope systematics of their constituent minerals, the xenoliths underwent metasomatism by a fluid in equilibrium with sediments in the fore-arc region of the subducting Farallon plate. The metasomatism resulted in the xenoliths acquiring distinctively different isotopic compositions from those of altered MORB despite their altered MORB protoliths; Sr and Pb have more radiogenic and Nd less radiogenic isotopic compositions than those of altered MORB. This suggests that basaltic oceanic crust with an isotopic composition reflecting metasomatism by a fluid in equilibrium with a sedimentary component can be introduced into the sub-arc mantle through subduction zones and could, therefore, explain the sediment-like isotopic signatures of some island arc basalt and ocean island basalts.

ACKNOWLEDGEMENTS

We are very grateful to S. Maruyama, G. E. Bebout and all of the PML members for their scientific guidance, technical support and valuable discussion. I. Buick and R. L. King are also acknowledged for improving the quality of this paper. We thank J. Selverstone, S. S. Sorensen and T. Zack for constructive reviews of this manuscript, and M. Wilson for editorial handling. This study was financially supported in part by grants from the Ministry of Education, Science, Sports and Culture of Japan (E.N.) and by the program 'Center of Excellence for the 21st Century in Japan' (E.N.).

REFERENCES

Aleinikoff, J. N., Dusel-Bacon, C., Foster, H. L. & Nokleberg, W. J. (1987). Lead isotopic fingerprinting of tectono-stratigraphic terranes, east–central Alaska. *Canadian Journal of Earth Sciences* **24**, 2089–2098.

Alt, J. C. (1995). Subseafloor processes in mid-ocean ridge hydrothermal systems. In: Humphris, S. E., Zierenberg, R. A., Mulineaux, L. S. & Thomson, R. E. (eds) *Seafloor Hydrothermal Systems: Physical, Chemical, Biological, and Geological Interactions. Geophysical Monograph, American Geophysical Union* **91**, 85–114.

Atherton, M. P. & Edmunds, W. M. (1966). An electron microprobe study of some zoned garnets from metamorphic rocks. *Earth and Planetary Science Letters* **1**, 185–193.

Atwater, T. (1970). Implications of plate tectonics for the Cenozoic tectonic evolution of Western North America. *Geological Society of America Bulletin* **81**, 3513–3536.

Ayers, J. C., Dittmer, S. K. & Layne, G. D. (1997). Partitioning of elements between peridotite and H_2O at 2·0–3·0 GPa and 900–1000°C, and application to models of subduction zone processes. *Earth and Planetary Science Letters* **150**, 381–398.

Bach, W., Peucker-Ehrenbrink, B., Hart, S. R. & Blusztajn, J. S. (2003). Geochemistry of hydrothermally altered oceanic crust: DSDP/ODP Hole 504B—implications for seawater–crust exchange budgets and Sr- and Pb-isotopic evolution of the mantle. *Geochemistry, Geophysics, Geosystems* **4**, doi:10.1029/2002GC000419.

Bebout, G. E. (1991). Field-based evidence for devolatilization in subduction zones: implications for arc magmatism. *Science* **251**, 413–416.

Becker, H., Jochum, K. P. & Carlson, R. W. (1999). Constraints from high-pressure veins in eclogites on the composition of hydrous fluids in subduction zones. *Chemical Geology* **160**, 291–308.

Becker, H., Jochum, K. P. & Carlson, R. W. (2000). Trace element fractionation during dehydration of eclogites from high-pressure terranes and the implications for element fluxes in subduction zones. *Chemical Geology* **163**, 65–99.

Bernard-Griffiths, J. & Cornichet, J. (1985). Origin of eclogites from south Brittany, France: a Sm–Nd isotopic and REE study. *Chemical Geology* **52**, 185–201.

Brenan, J. M., Shaw, H. F., Phinney, D. L. & Ryerson, F. J. (1994). Rutile–aqueous fluid partitioning of Nb, Ta, Hf, Zr, U and Th:

implications for high field strength element depletions in island-arc basalts. *Earth and Planetary Science Letters* **128**, 327–339.

Brenan, J. M., Shaw, H. F., Ryerson, F. J. & Phinney, D. L. (1995). Mineral–aqueous fluid partitioning of trace elements at 900°C and 2·0 GPa: constraints on the trace element chemistry of mantle and deep crustal fluids. *Geochimica et Cosmochimica Acta* **59**, 3331–3350.

Brenan, J. M., Ryerson, F. J. & Shaw, H. F. (1998). The role of aqueous fluids in the slab-to-mantle transfer of boron, beryllium, and lithium during subduction: experiments and models. *Geochimica et Cosmochimica Acta* **62**, 3337–3343.

Bröcker, M. & Enders, M. (2001). Unusual bulk-rock compositions in eclogite-facies rocks from Syros and Tinos (Cyclades, Greece): implications for U–Pb zircon geochronology. *Chemical Geology* **175**, 581–603.

Caron, J.-M. & Pèquignot, G. (1986). The transition between blueschists and lawsonite-bearing eclogite based on observations from Corsican metabasalts. *Lithos* **19**, 205–218.

Carswell, D. A. (1990). Eclogite and the eclogite facies: definitions and classification. In: Carswell, D. A. (ed.) *Eclogite Facies Rocks*. New York: Chapman and Hall, 396 pp.

Catanzaro, E. J., Murphy, T. J., Shields, W. R. & Garner, E. L. (1968). Absolute isotopic abundance ratios of common, equal-atom, and radiogenic lead isotopic standards. *Journal of Research of the National Bureau of Standards* **72A**, 261–267.

Cherniak, D. J. (2001). Pb diffusion in Cr diopside, augite, and enstatite, and consideration of the dependence of cation diffusion in pyroxene on oxygen fugacity. *Chemical Geology* **177**, 381–397.

Church, S. E. & Tatsumoto, M. (1975). Lead isotope relations in oceanic ridges basalts from the Juan de Fuca–Gorda Ridge Area, N. E. Pacific Ocean. *Contributions to Mineralogy and Petrology* **53**, 253–279.

Clement, C. R., Skinner, E. M. W. & Smith, B. H. S. (1984). Kimberlite redefined. *Journal of Geology* **92**, 223–228.

Condie, K. C. (1982). Plate-tectonics model for Proterozoic continental accretion in the southwestern United States. *Geology* **10**, 37–42.

Coney, P. J. & Reynolds, S. (1977). Cordilleran Benioff zones. *Nature* **270**, 403–406.

David, K., Schiano, P. & Allègre, C. J. (2000). Assessment of the Zr/Hf fractionation in oceanic basalts and continental materials during petrogenetic processes. *Earth and Planetary Science Letters* **178**, 285–301.

Deer, W. A., Howie, R. A. & Zussman, J. (1992). *An Introduction to the Rock-Forming Minerals*. Harlow: Longman.

DePaolo, D. J., Linn, A. M. & Schubert, G. (1991). The continental age distribution: methods of determining mantle separation ages from Sm–Nd isotopic data and application to the southwestern U.S. *Journal of Geophysical Research* **96**, 2071–2088.

Dickinson, W. R. (1997). Tectonic implications of Cenozoic volcanism in coastal California. *Geological Society of America Bulletin* **109**, 936–954.

Ehrenberg, S. N. (1982). Petrogenesis of garnet lherzolite and megacrystalline nodules from the Thumb, Navajo volcanic field. *Journal of Petrology* **23**, 507–547.

Ernst, W. G. (1970). Tectonic contact between the Franciscan mélange and the Great Valley Sequence—crustal expression of a late Mesozoic Benioff Zone. *Journal of Geophysical Research* **75**, 886–901.

Essene, E. J. & Fyfe, W. S. (1967). Omphacite in California metamorphic rocks. *Contributions to Mineralogy and Petrology* **15**, 1–23.

Farmer, G. L., Ayuso, R. & Plafker, G. (1993). A Coast Mountains provenance for the Valdez and Orca groups, southern Alaska, based on Nd, Sr, and Pb isotopic evidence. *Earth and Planetary Science Letters* **116**, 9–21.

Farquhar, J., Chacko, T. & Ellis, D. J. (1996). Preservation of oxygen isotope compositions in granulites from Northwestern Canada and Enderby Land, Antarctica: implications for high-temperature isotopic thermometry. *Contributions to Mineralogy and Petrology* **125**, 213–224.

Gao, J. & Klemd, R. (2001). Primary fluids entrapped at blueschist to eclogite transition: evidence from the Tianshan meta-subduction complex in northwestern China. *Contributions to Mineralogy and Petrology* **142**, 1–14.

Hamilton, W. (1969). Mesozoic California and the underflow of Pacific mantle. *Geological Society of America Bulletin* **80**, 2409–2430.

Hart, S. (1984). A large-scale isotope anomaly in the Southern Hemisphere mantle. *Nature* **309**, 753–757.

Hegner, E. & Tatsumoto, M. (1987). Pb, Sr, and Nd isotopes in basalts and sulfides from the Juan de Fuca ridge. *Journal of Geophysical Research* **92**, 11380–11386.

Helmstaedt, H. & Doig, R. (1975). Eclogite nodules from kimberlite pipes of the Colorado Plateau—samples of subducted Franciscan-type oceanic lithosphere. *Physics and Chemistry of the Earth* **9**, 95–112.

Helmstaedt, H. & Schulze, D. J. (1988). Eclogite-facies ultramafic xenolith from Colorado Plateau diatreme breccias: composition with eclogites in crustal environments, evaluation of the subduction hypothesis, and implications for eclogite xenoliths from diamondiferous kimberlites. In: Smith, D. C. (ed.) *Eclogites and Eclogite-Facies Rocks*. New York: Elsevier, pp. 387–450.

Helmstaedt, H. H. & Schulze, D. J. (1991). Early to Mid-Tertiary inverted metamorphic gradient under the Colorado Plateau: evidence from eclogite xenoliths in ultramafic microbreccias, Navajo volcanic field. *Journal of Geophysical Research* **96**, 13225–13235.

Hofmann, A. W. (1997). Mantle geochemistry: the message from oceanic volcanism. *Nature* **385**, 219–229.

Iizuka, Y. & Nakamura, E. (1995). Experimentally study of the slab–mantle interaction and implications for the formation of titanoclinohumite at deep subduction zone. *Proceedings of the Japan Academy* **71**, 159–164.

Ishikawa, T. & Nakamura, E. (1994). Origin of the slab component in arc lavas from across-arc variation of B and Pb isotopes. *Nature* **370**, 205–208.

Jahn, B.-M., Cornichet, J., Cong, B. & Yui, T.-F. (1996). Ultrahigh-εNd eclogites from an ultrahigh-pressure metamorphic terrane of China. *Chemical Geology* **127**, 61–79.

Kelley, S. P. & Wartho, J. A. (2000). Rapid kimberlite ascent and the significance of Ar–Ar ages in xenolith phlogopites. *Science* **289**, 609–611.

Kogiso, T., Tatsumi, Y. & Nakano, S. (1997). Trace element transport during dehydration process in the subducted oceanic crust: 1. Experiments and implications for the origin of ocean island basalts. *Earth and Planetary Science Letters* **148**, 193–205.

Kuritani, T. & Nakamura, E. (2002). Precise isotope analysis of nanogram-level Pb for natural rock samples without use of double spikes. *Chemical Geology* **186**, 31–43.

Kuritani, T. & Nakamura, E. (2003). High precise and accurate isotopic analysis of small amounts of Pb using ^{205}Pb–^{204}Pb and ^{207}Pb–^{204}Pb, two double spikes. *Journal of Analytical Atomic Spectrometry* **18**, 1464–1470.

Makishima, A. & Nakamura, E. (1991). Precise measurement of cerium isotope composition in rock samples. *Chemical Geology* **94**, 1–11.

Makishima, A. & Nakamura, E. (1997). Suppression of matrix effect in ICP-MS by high power operation of ICP: application to precise determination of Rb, Sr, Y, Cs, Ba, REE, Pb, Th, and U at ng g^{-1} levels in milligram silicate samples. *Geostandards Newsletter*.

Makishima, A., Nakamura, E. & Nakano, T. (1999). Determination of zirconium, niobium, hafnium and tantalum at ng g^{-1} levels in geological materials by direct nebulisation of sample HF solution into Fl-ICP-MS. *Geostandards Newsletter* **23**, 7–20.

Maruyama, S. & Liou, J. G. (1988). Petrology of Franciscan metabasites along the jadeite–glaucophane type facies series, Cazadero, California. *Journal of Petrology* **29**, 1–37.

Maruyama, S. & Liou, J. G. (1989). Possible depth limit for underplating by a seamount. *Tectonophysics* **160**, 327–337.

McCulloch, M. T. & Gamble, J. A. (1991). Geochemical and geodynamical constraints on subduction zone magmatism. *Earth and Planetary Science Letters* **102**, 358–374.

McGetchin, T. R., Smith, D. C., Ehrenberg, S. N., Roden, M. & Wilshire, H. G. (1977). *Navajo Kimberlite and Minette Guide. Second International Kimberlite Conference Field Excursion Guide. Santafe, NM.* Washington, DC: American Geophysical Union, 40 pp.

Moore, D. E. & Liou, J. G. (1979). Mineral chemistry of some Franciscan blueschist metasediments from the Diablo Range, California Part I. *Geological Society of America Bulletin* **90**, 1089–1091.

Moriguti, T., Makishima, A. & Nakamura, E. (2004). Determination of lithium contents in silicates by isotope dilution ICP-MS and its evaluation by isotope dilution thermal ionisation mass spectrometry. *Geostandards Newsletter* **28**, 371–382.

Naeser, C. W. (1971). Geochronology of the Navajo–Hopi Diatremes, Four Corners Area. *Journal of Geophysical Research* **76**, 4978–4985.

Nakamura, E. & Kushiro, I. (1998). Trace element diffusion in jadeite and diopside melt at high pressure and its geochemical implication. *Geochimica et Cosmochimica Acta* **62**, 3151–3160.

Nakamura, E., Makishima, A., Moriguti, T., Kobayashi, K., Sakaguchi, C., Yokoyama, T., Tanaka, R., Kuritani, T. & Takei, H. (2002). Comprehensive geochemical analyses of small amounts (<100 mg) of extraterrestrial samples for the analytical competition related to the sample-return mission, MUSES-C. *The Institute of Space and Astronautical Science Report* 16.

Nakano, T. & Nakamura, E. (1998). Static multicollection of $Cs_2BO_2^+$ ions for precise boron isotope analysis with positive thermal ionization mass spectrometry. *International Journal of Mass Spectrometry and Ion Processes* **176**, 13–21.

Okamoto, K. & Maruyama, S. (1999). The high-pressure synthesis of lawsonite in MORB + H_2O system. *American Mineralogist* **94**, 362–373.

Peacock, S. M. (1993). The importance of blueschist–eclogite dehydration reactions in subducting oceanic crust. *Geological Society of America Bulletin* **105**, 684–694.

Poli, S. & Schmidt, M. W. (2002). Petrology of subducted slabs. *Annual Review of Earth and Planetary Sciences* **30**, 207–235.

Roden, M. F. (1981). Origin of coexisting minette and ultramafic breccia, Navajo Volcanic Field. *Contributions to Mineralogy and Petrology* **77**, 195–206.

Roden, M. F., Smith, D. & McDowell, F. W. (1979). Age and extent of potassic volcanism on the Colorado Plateau. *Earth and Planetary Science Letters* **43**, 279–284.

Roden, M. F., Smith, D. & Murthy, V. R. (1990). Chemical constraints on lithosphere composition and evolution beneath the Colorado Plateau. *Journal of Geophysical Research* **95**, 2811–2831.

Scambelluri, M. & Philippot, P. (2001). Deep fluids in subduction zones. *Lithos* **55**, 213–227.

Schmidt, M. W. & Poli, S. (1998). Experimentally based water budgets for dehydrating slabs and consequences for arc magma generation. *Earth and Planetary Science Letters* **163**, 361–379.

Selverstone, J., Pun, A. & Condie, K. C. (1999). Xenolithic evidence for Proterozoic crustal evolution beneath the Colorado Plateau. *Geological Society of America Bulletin* **111**, 590–606.

Shibata, T. & Nakamura, E. (1997). Across arc variation of isotope and trace element compositions from Quaternary basaltic volcanic rocks in northeastern Japan: implication for interaction between subducted oceanic slab and mantle wedge. *Journal of Geophysical Research* **102**, 8051–8064.

Shreve, R. L. & Cloos, M. (1986). Dynamics of sediment subduction, mélange formation, and prism accretion. *Journal of Geophysical Research* **91**, 10229–10245.

Smith, D. & Levy, S. (1976). Petrology of the Green Knobs diatreme and implications for the upper mantle below the Colorado Plateau. *Earth and Planetary Science Letters* **29**, 107–125.

Smith, D. & Zientek, M. (1979). Mineral chemistry and zoning in eclogite inclusions from Colorado Plateau diatremes. *Contributions to Mineralogy and Petrology* **69**, 119–131.

Smith, D., Connelly, J. N., Manser, K., Moser, D. E., Housh, T. B., McDowell, F. W. & Mack, L. E. (2004). Evolution of Navajo eclogites and hydration of the mantle wedge below the Colorado Plateau, southwestern United States. *Geochemistry, Geophysics, Geosystems* **5**, 2003GC000675.

Sneeringer, M., Hart, S. R. & Shimizu, N. (1984). Strontium and samarium diffusion in diopside. *Geochimica et Cosmochimica Acta* **48**, 1589–1609.

Sorensen, S. S. (1988). Petrology of amphibolite-facies mafic and ultramafic rocks from the Catalina Schist, southern California: metasomatism and migmatization in a subduction zone metamorphic setting. *Journal of Metamorphic Geology* **6**, 405–435.

Sorensen, S. S. (1991). Petrogenetic significance of zoned allanite in garnet amphibolites from a paleo-subduction zone: Catalina Schist, southern California. *American Mineralogist* **76**, 589–601.

Sorensen, S. S. & Grossman, J. N. (1989). Enrichment of trace elements in garnet amphibolites from a paleo-subduction zone: Catalina Schist, southern California. *Geochimica et Cosmochimica Acta* **53**, 3155–3177.

Sorensen, S. S. & Grossman, J. N. (1993). Accessory minerals and subduction zone metasomatism: a geochemical comparison of two mélanges (Washington and California, U.S.A.). *Chemical Geology* **110**, 269–297.

Spandler, C., Hermann, J., Richard, A. & Mavrogenes, J. (2003). Redistribution of trace elements during prograde metamorphism from lawsonite blueschist to eclogite facies; implications for deep subduction-zone processes. *Contributions to Mineralogy and Petrology* **146**, 205–222.

Stalder, R., Foley, S. F., Brey, G. P. & Horn, I. (1998). Mineral–aqueous fluid partitioning of trace elements at 900–1200°C and 3·0–5·7 GPa: new experimental data for garnet, clinopyroxene, and rutile, and implications for mantle metasomatism. *Geochimica et Cosmochimica Acta* **62**, 1781–1801.

Stracke, A., Bizimis, M. & Salters, V. J. M. (2003). Recycling oceanic crust: quantitative constraints. *Geochemistry, Geophysics, Geosystems* **4**, doi: 10.1029/2001GC000223.

Sun, S. S. & McDonough, W. F. (1989). Chemical and isotopic systematics of oceanic basalt: implications for mantle composition and process. In: Sun, S. S. & McDonough, W. F. (eds) *Magmatism in the Ocean Basins. Geological Society, London, Special Publications* **42**, 313–345.

Takei, H. (2002). Development of precise analytical techniques for major and trace element concentrations in rock samples and their applications to the Hishikari Gold Mine, southern Kyushu, Japan. PhD thesis, Okayama University.

Taylor, R. N. & Nesbitt, R. W. (1998). Isotopic characteristics of subduction fluids in intra-oceanic setting, Izu–Bonin Arc, Japan. *Earth and Planetary Science Letters* **164**, 79–98.

Thöni, M. & Jagoutz, E. (1992). Some new aspects of dating eclogites in orogenic belts: Sm–Nd, Rb–Sr, and Pb–Pb isotopic results from the Austroalpine Saualpe and Koralpe type-locality (Carinthia/Styria, southeastern Austria). *Geochimica et Cosmochimica Acta* **56**, 347–368.

Tilton, G., Ames, L., Schertl, H. P. & Schreyer, W. (1997). Reconaissance isotopic investigations on rocks of an undeformed granite contact within the coesite-bearing unit of the Dora Maira Massif. *Lithos* **41**, 25–36.

Tribuzio, R., Messiga, B., Vannucci, R. & Bottazzi, P. (1996). Rare earth element redistribution during high-pressure–low-temperature metamorphism in ophiolitic Fe-gabbros (Liguria, northwestern Italy): implications for light REE mobility in subduction zones. *Geology* **24**, 711–714.

Tual, E., Jahn, B. M., Bougault, H. & Joron, J. L. (1985). Geochemistry of basalts from hole 504B, leg 83, Costa Rica rift. In: Anderson, R. N., Honnorez, J., *et al.* (eds) *Initial Reports of the Deep Sea Drilling Project, 83*. Washington, DC: US Government Printing Office, pp. 201–214.

Usui, T. (2004). A geochemical study of the origin of eclogite xenoliths from the Colorado Plateau, southwestern United States: implications for the evolution of subducted oceanic crust. PhD thesis, Okayama University.

Usui, T., Kobayashi, K. & Nakamura, E. (2002). U–Pb isotope systematics of micro-zircon inclusions: implications for the age and origin of eclogite xenolith from the Colorado Plateau. *Proceedings of the Japan Academy* **78**, 51–56.

Usui, T., Nakamura, E., Kobayashi, K., Maruyama, S. & Helmstaedt, H. (2003). Fate of the subducted Farallon plate inferred from eclogite xenoliths in the Colorado Plateau. *Geology* **31**, 589–592.

van Keken, P. E., Hauri, E. H. & Ballentine, C. J. (2002). Mantle mixing: the generation, preservation, and destruction of chemical heterogeneity. *Annual Review of Earth and Planetary Sciences* **30**, 493–525.

van Orman, J. A., Grove, T. L. & Shimizu, N. (1998). Rare earth element diffusion in diopside and disequilibrium melting in the mantle. *EOS Transactions, American Geophysical Union* **79**, S371.

Wasserburg, G. J., Jacobsen, S. B., DePaolo, D. J., McCulloch, M. T. & Wen, T. (1981). Precise determination of Sm/Nd ratios, Sm and Nd isotopic abundances in standard solutions. *Geochimica et Cosmochimica Acta*, **45**, 2311–2323.

Wendlandt, E., DePaolo, D. J. & Baldridge, S. W. (1993). Nd and Sr isotope chronostratigraphy of Colorado Plateau lithosphere: implications for magmatic and tectonic underplating of the continental crust. *Earth and Planetary Science Letters* **116**, 23–43.

White, W. M., Hofmann, A. W. & Puchelt, H. (1987). Isotope geochemistry of Pacific mid-ocean ridge basalt. *Journal of Geophysical Research* **92**, 4881–4893.

Yokoyama, T., Makishima, A. & Nakamura, E. (1999). Separation of thorium and uranium from silicate rock samples using two commercial extraction chromatographic resins. *Analytical Chemistry* **71**, 135–141.

Yokoyama, T., Kobayashi, K., Kuritani, T. & Nakamura, E. (2003). Mantle metasomatism and rapid ascent of slab components beneath island arcs: evidence from ^{238}U–^{230}Th–^{226}Ra disequilibria of Miyakejima volcano, Izu arc, Japan. *Journal of Geophysical Research* **108**(B7), doi: 10.1029/2002JB002103.

Yoshikawa, M. & Nakamura, E. (1993). Precise isotope determination of trace amounts of Sr in magnesium-rich samples. *Journal of Mineralogy, Petrology and Economic Geology* **88**, 548–561.

Zack, T., Foley, S. F. & Rivers, T. (2002*a*). Equilibrium and disequilibrium trace element partitioning in hydrous eclogites (Trescolmen, Central Alps). *Journal of Petrology* **43**, 1947–1974.

Zack, T., Kronz, A., Foley, S. F. & Rivers, T. (2002*b*). Trace element abundances in rutiles from eclogites and associated garnet mica schists. *Chemical Geology* **184**, 97–122.

Zack, T., Tomascak, P. B., Rudnick, R. L., Dalpé, C. & McDonough, W. F. (2003). Extremely light Li in orogenic eclogites: the role of isotope fractionation during dehydration in subducted oceanic crust. *Earth and Planetary Science Letters* **208**, 279–290.

Zack, T., Rivers, T., Brumm, R. & Kronz, A. (2004). Cold subduction of oceanic crust: implications from a lawsonite eclogite from Dominican Republic. *European Journal of Mineralogy* **16**, 909–916.

Zindler, A. & Hart, S. (1986). Chemical geodynamics. *Annual Review of Earth and Planetary Sciences* **14**, 493–571.

Zuleger, E., Alt, J. C. & Erzinger, J. (1995). Primary and secondary variations in major and trace element geochemistry of the lower sheeted dike complex: hole 504B, leg 140. In: Becker, K., Graham, A. G., *et al.* (eds) *Proceedings of the Ocean Drilling Program, Scientific Results, 137/140*. College Station, TX: Ocean Drilling Program, pp. 65–80.

APPENDIX

Table A1: Repeat analyses for Sr–Nd–Pb isotopic compositions and abundances of Rb, Sr, Sm, Nd, U, Th and Pb (ppm) in standard rock (JB3)

	Sample					Average	2σ	Reference data*	2σ
	1	2	3	4	5				
Rb	14·087	14·085	14·143	14·141	14·144	14·120	0·062	13·92	0·28
$2\sigma_{mean}$	0·015	0·050	0·008	0·010	0·007				
Sr	411·32	411·62	411·14	411·75	410·81	411·33	0·76	409·97	1·05
$2\sigma_{mean}$	0·06	0·06	0·04	0·06	0·05				
$^{87}Sr/^{86}Sr$	0·703343	0·703384	0·703357	0·703367	0·703358	0·703362	0·000031	0·703393	0·000009
$2\sigma_{mean}$	0·000006	0·000007	0·000007	0·000008	0·000008				
Sm	4·260	4·246	4·234	4·249	4·242	4·246	0·020	4·237	0·005
$2\sigma_{mean}$	0·018	0·011	0·010	0·011	0·011				
Nd	15·6278	15·6405	15·6422	15·6450	15·6289	15·637	0·016	15·583	0·051

Table A1: Continued

	Sample					Average	2σ	Reference data*	2σ
	1	2	3	4	5				
$2\sigma_{mean}$	0·0007	0·0007	0·0007	0·0008	0·0006				
$^{143}Nd/^{144}Nd$	0·513053	0·513061	0·513036	0·513056	0·513053	0·513052	0·000018	0·513060	0·000010
$2\sigma_{mean}$	0·000005	0·000007	0·000007	0·000006	0·000006				
U	0·4773	0·4766	0·4759	0·4751	0·4774	0·4765	0·0019	0·4753	0·0006
$2\sigma_{mean}$	0·0016	0·0014	0·0016	0·0019	0·0005				
Th	1·275	1·273	1·278	1·277	1·275	1·275	0·004	1·271	0·006
$2\sigma_{mean}$	0·002	0·001	0·001	0·001	0·001				
Pb	5·029	5·028	5·034	5·049	5·035	5·035	0·017	5·035	0·008
$^{206}Pb/^{204}Pb$	18·298	18·294	18·295	18·297	18·293	18·295	0·004	18·299	0·002
$^{207}Pb/^{204}Pb$	15·540	15·537	15·537	15·541	15·536	15·538	0·004	15·541	0·002
$^{208}Pb/^{204}Pb$	38·257	38·248	38·248	38·258	38·246	38·251	0·011	38·258	0·007

*Reference data are from Kuritani & Nakamura (2003) for Pb isotope compositions, Yokoyama *et al*. (2003) for U and Th abundances, and C. Sakaguchi (personal communications). JB3 is a basaltic rock standard (from Mt. Fuji) supplied by the Geological Survey of Japan.